AD-A125 648 CALCULATIONS OF THREE-DIMENSIONAL TURBULENT BOUNDARY LAYERS USING THE CRA..(U) IOWA INST OF HYDRAULIC RESEARCH IOWA CITY P A KROGSTAD ET AL. AUG 82 IIHR-254 1/1

UNCLASSIFIED N00014-82-K-0200 F/G 20/4 NL

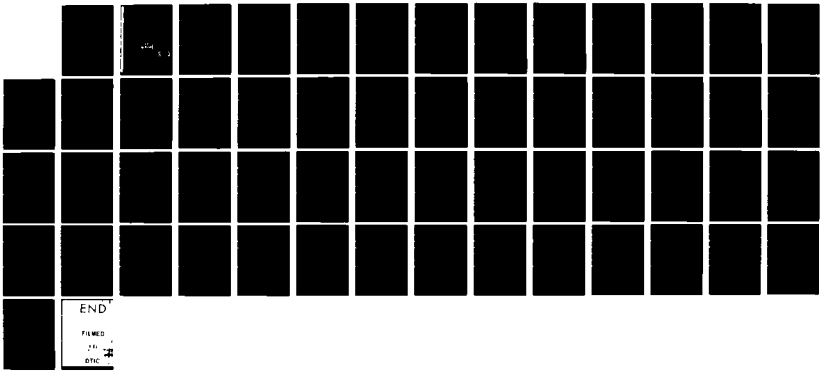

END

FILMED

DTIC

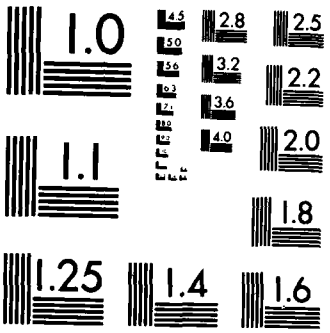

(12)

CALCULATIONS OF THREE-DIMENSIONAL TURBULENT BOUNDARY LAYERS USING THE CRANK-NICOLSON METHOD

by

P. A. Krogstad, J. H. Baek, and V. C. Patel

A report on the calculations presented at the
EUROVISC WORKSHOP ON 3D BOUNDARY LAYERS
Berlin, April 1982

Sponsored by
General Hydromechanics Research Program
of the Naval Sea Systems Command
Naval Ship Research and Development Center
Contract No. N00014-82-K0200

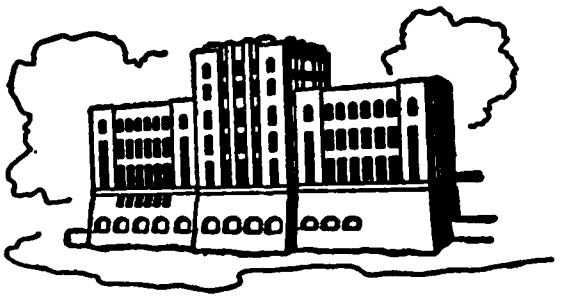

IIHR Report No. 254

Iowa Institute of Hydraulic Research
The University of Iowa
Iowa City, Iowa 52242

August 1982

CALCULATIONS OF THREE-DIMENSIONAL TURBULENT BOUNDARY LAYERS USING THE CRANK-NICOLSON METHOD

by

P. A. Krogstad, J. H. Baek, and V. C. Patel

A report on the calculations presented at the
EUROVISC WORKSHOP ON 3D BOUNDARY LAYERS
Berlin, April 1982

Sponsored by
General Hydromechanics Research Program
of the Naval Sea Systems Command
Naval Ship Research and Development Center
Contract No. N00014-82-K0200

IIHR Report No. 254

Iowa Institute of Hydraulic Research
The University of Iowa
Iowa City, Iowa 52242

August 1982

REPORT DOCUMENTATION PAGE

READ INSTRUCTIONS BEFORE COMPLETING FORM

1. REPORT NUMBER	2. GOVT ACCESSION NO. A125 648 / 3. RECIPIENT'S CATALOG NUMBER
4. TITLE (and Subtitle) Calculations of Three-Dimensional Turbulent Boundary Layers Using the Crank-Nicolson Method	5. TYPE OF REPORT & PERIOD COVERED Final Oct 1980 - Aug 1982
	6. PERFORMING ORG. REPORT NUMBER IIHR Report No. 254
7. AUTHOR(s) P.A. Krogstad, J.H. Baek and V.C. Patel	8. CONTRACT OR GRANT NUMBER(s) N00014-82-K0200
9. PERFORMING ORGANIZATION NAME AND ADDRESS Iowa Institute of Hydraulic Research, The University of Iowa, Iowa City, Iowa 52242	10. PROGRAM ELEMENT, PROJECT, TASK AREA & WORK UNIT NUMBERS
11. CONTROLLING OFFICE NAME AND ADDRESS David W. Taylor Naval Ship Research and Development Center, Bethesda, Maryland 20084	12. REPORT DATE August 1982 13. NUMBER OF PAGES
14. MONITORING AGENCY NAME & ADDRESS (if different from Controlling Office)	15. SECURITY CLASS. (of this Report) UNCLASSIFIED 15a. DECLASSIFICATION/DOWNGRADING SCHEDULE

16. DISTRIBUTION STATEMENT (of this Report)

Approved for Public Release, Distribution Unlimited

17. DISTRIBUTION STATEMENT (of the abstract entered in Block 20, if different from Report)

18. SUPPLEMENTARY NOTES

19. KEY WORDS (Continue on reverse side if necessary and identify by block number)

Boundary Layers, Three-Dimensional, Turbulent, Calculations, Finite-Difference Methods

20. ABSTRACT (Continue on reverse side if necessary and identify by block number)

This report describes the results of the three-dimensional turbulent boundary-layer calculations performed for the Eurovisc Workshop held in Berlin on 1 April 1982. It is shown that the present method, based on the Crank-Nicolson finite-difference scheme and a simple eddy-viscosity model for turbulence, yields satisfactory results provided regions of viscous-inviscid interaction, which were present in at least three of the four test cases, are avoided.

I. INTRODUCTION

Many competing methods have been developed over the past two decades for the calculation of turbulent boundary layers. Most earlier methods were restricted to two-dimensional flow, and these were evaluated at the Stanford Conference of 1968 (Kline et al, 1968) by comparing their predictions with a large number of carefully selected experimental data sets. Some of the promising methods have since been extended for application to three-dimensional turbulent boundary layers and a few new ones have been developed. In recent years, attempts have been made to assess the state of the art in three-dimensional boundary-layer calculations through a series of workshops: Eurovisc in Trondheim, 1975 (East, 1975; Fannelop and Krogstad, 1975), the Stockholm Workshop, 1978 (Humphreys, 1979), the Amsterdam Workshop, 1980 (Lindhout, van den Berg and Elsenaar, 1981) and the SSPA-ITTC Workshop on Ship Boundary Layers, 1980 (Larsson, 1981). A limited number of test cases was chosen at each and comparisons were made with the predictions by different methods.

The Eurovisc Workshop, held in Berlin on 1 April 1982, invited participants to compute five test cases, three of which were "recommended" by the organizers and the remaining two were considered "optional". The specifications of the initial and boundary conditions, and the output information and format were provided to the participants (Humphreys, 1981). The number of test cases computed by the 13 participants at the workshop ranged from only one solved by two participants to a maximum of four. The findings of the workshop will be reported in the forthcoming proceedings.

The purpose of this report is to describe the Institute's entry, which consisted of calculations for four test cases. The simpler of the two methods developed at the Institute, namely the Crank-Nicolson method of Chang and Patel (1975), was utilized since the test cases did not demand the additional capabilities of the more advanced ADI method of Patel and Choi (1978). This report provides an outline of the method and a description of the calculations and results, pointing out some of the peculiar features in each test case.

All the results presented have been scaled by the scaling factors specified by the organizers. These scales are constants and represent some

characteristic length scales of the experiments. Thus, the scaling of velocity and shear-stress profiles with the boundary layer thickness, which tends to hide differences between calculations and measurements, is avoided.

II. OUTLINE OF THE CRANK-NICOLSON METHOD

This method solves the usual three-dimensional, thin boundary-layer equations for laminar and turbulent flows. The computer program can execute solutions in any curvilinear, orthogonal, surface-fitted coordinates and contains options to perform calculations for two-dimensional, plane-of-symmetry and infinite-yawed-cylinder flows, in addition to fully three-dimensional boundary layers. A detailed description of the method and some applications to laminar and turbulent boundary layers are given in Chang and Patel (1975), a listing of the computer program is contained in Choi (1978) and some recent applications to the boundary layer on bodies of revolution at incidence are presented in Patel and Choi (1978) and Patel and Baek (1982).

For turbulent flow, the two Reynolds stresses in the momentum equations are related to the mean-velocity field by means of the two-layer isotropic eddy-viscosity model of Cebeci and Smith (see Cebeci and Bradshaw, 1977). The model incorporates the "low Reynolds number" and "pressure gradient" effects through changes in the van Driest damping constant and also attempts to mimic transition from laminar to turbulent flow by means of an intermittency function. Solid boundaries do not require special treatment since the equations are solved upto the wall. Unless noted otherwise, the various constants and functions in the eddy-viscosity model are the same as those originally proposed.

The well known Crank-Nicolson scheme is used to discretize the differential equations. In the two momentum equations, central differences are employed in the secondary- and main-flow directions. Thus, the truncation errors are of the second order. In the continuity equation, the normal derivative is approximated by a central-difference formula but two-point backward differences are used for those in the other two directions. The

overall accuracy of the numerical scheme is therefore less than that of a completely second-order scheme.

The computation domain in the direction normal to the surface extends from the wall, where the no-slip condition applies, to some distance beyond the edge of the boundary layer, where the velocity components approach their potential-flow values. Typically, 25 to 40 grid points are distributed nonuniformly across this domain. Additional grid points are added at the outer edge as the boundary layer grows to insure that the whole boundary layer lies within the integration domain.

The step size in the cross-stream direction may be chosen arbitrarily and need not be constant. The choice is dictated primarily by the rate of change quantities, such as the boundary-layer thickness, in that direction. The step size in the primary direction is subject to the CFL stability criterion. Extensive numerical tests performed earlier indicate that step sizes of the order of two to three boundary-layer thicknesses give accurate grid-independent solutions for most cases, but smaller steps are needed if calculations proceed into regions of rapid boundary-layer growth.

The finite-difference equivalents of the momentum equations are solved first to determine the velocity components parallel to the surface. These equations are linearized using the procedure of Flugge-Lotz and Blottner. The continuity equation is then solved for the normal component. The solutions are iterated to convergence. Two to three iterations are required to account for the nonlinearity of the momentum equations.

The solutions march along the secondary- and primary-flow directions. In its present form, therefore, the method cannot handle reversals in the secondary-flow velocity.

In order to perform a calculation for the three-dimensional boundary layer, the method requires the specification of the two components of velocity outside the boundary layer. If only the surface pressure distribution is known, a separate program is utilized to trace the external streamlines and determine the external velocity components.

The initial and boundary conditions employed in each of the test cases are described below.

III. TEST CASES

1. Infinite-Yawed Wing, BEEL72

1.1 Description of the problem. The first of the recommended test cases was the infinite-swept wing experiment carried out at NLR, Amsterdam, by van den Berg and Elsenaar (1972) and Elsenaar and Boelsma (1974). The geometry is shown in figure 1.1. It consists of a flat surface swept at 35°. A wing type body was mounted above the flat surface to produce a streamwise pressure gradient on the test surface. Extreme care was taken to produce as close to infinite-swept-wing conditions as possible by use of side vanes. The measured pressure field showed only a small spanwise variation.

Because of the infinite-swept-wing configuration, the problem is quasi two-dimensional. If Cartesian coordinates are used (see figure 1.1) the boundary-layer equations are reduced to

$$U\frac{\partial U}{\partial x} + V\frac{\partial U}{\partial y} = -\frac{1}{\rho}\frac{\partial p}{\partial x} + \frac{1}{\rho}\frac{\partial \tau_{xy}}{\partial y}$$

$$U\frac{\partial W}{\partial x} + V\frac{\partial W}{\partial y} = \frac{1}{\rho}\frac{\partial \tau_{zy}}{\partial y} \qquad (1.1)$$

$$\frac{\partial U}{\partial x} + \frac{\partial V}{\partial y} = 0$$

Therefore, the coupling between the two momentum equations occurs only through the turbulent part of the shear stresses. At the edge of the boundary layer, the momentum equations reduce to

$$U_e\frac{\partial U_e}{\partial x} = \frac{1}{\rho}\frac{\partial p}{\partial x}$$

$$\frac{\partial W_e}{\partial x} = 0 \qquad \text{or} \qquad W_e = \text{const.}$$

Using these, the distributions of U_e and W_e could be derived from the measured streamwise pressure distribution which was supplied by the organizers. In addition to the pressure field, the measured velocity and shear-stress profiles at the starting point were supplied. However, since the present

method models the turbulent stresses by an eddy-viscosity assumption, only the velocity profile is required. This profile had a number of shortcomings. First, the profile did not go monotomically to the freestream velocity but showed a series of wiggles at the outer edge. When used in the program, these wiggles were not damped out but continued to grow in the U and W profiles. Second, the program requires the first profile point to be within $y^+ < 4$ whereas the first measured point was at $y^+ \sim 14.6$. A new profile was therefore generated from van Driest's law of the wall and Coles' wake function, using the measured C_f, θ and U_e.

Since it is the derivative of the pressure that enters the governing equations, care should be taken when experimental pressure fields are entered because these will never be perfectly smooth. This was also found to be the case in this experiment and a moderate smoothing of the pressure data was therefore performed. The pressure was then spline-fitted allowing C_{pw} to be computed at any chordwise location.

These calculations were performed by marching the solution normal to the leading edge (x,z-system) from x = 0.52 m. However, since the results were required in streamline coordinates (velocity profiles and integral variables) as well as in the tunnel-axis coordinate system (x',z') (for shear-stress profiles), some coordinate transformations were necessary in the presentation of the final results. This case was calculated using the infinite-yawed-cylinder-flow option in the program. A total of 119 streamwise steps and 40 grid points perpendicular to the wall were used.

1.2 Results. Figure 1.2 shows how the angle between the wall streamline (surface shear) and the tunnel axis changes with streamwise distance. This angle is the sum of the freestream angle with respect to the tunnel axis and the boundary-layer crossflow angle at the wall. Separation occurs when the sum of these two angles equals $\pi-\lambda = 55^0$ where λ is the sweep angle of 35°. For the initial profile at x = 0.52m, the wall crossflow angle was 1.5° and the freestream angle 4°. Both the wall crossflow and the freestream angles increase monotonically and separation was observed experimentally at x = 1.32m where the wall crossflow angle was 38.9° and the freestream angle was 16.1°. As seen from the figure, separation was not predicted in the calculations. In

fact none of the calculations presented at the workshop predicted separation. This was, however, not surprising because the same result was found in the "Trondheim Trials" (East, 1975). Most methods agreed with the experiment up to about x = 1.05m, but failed to predict the rapid increase in wall crossflow angle and growth of boundary layer thickness (figure 1.3) found in the experiments. Also, the agreement between the predicted and measured skin-friction coefficient was limited to the upstream region, although the deviations were not so severe (figure 1.4). The reason for the disagreement could either be strong viscous-inviscid interaction over a substantial region upstream of separation or that the inifinite-swept-wing conditions were not satisfied exactly.

Viscous-inviscid interaction effects are usually restricted to about one or two boundary-layer thicknesses upstream of the separation line (see, for example, the calculations of the DEFE77 test case). However, in this experiment the interaction is felt about six boundary-layer thicknesses upstream. It should be pointed out that the wall crossflow angle is very sensitive to the streamwise pressure gradient and some participants demonstrated that considerable improvements in the results could be obtained by slightly increasing the pressure gradient beyond $x \approx 1$ m. Another approach applied was the so-called inverse method where the distribution of one of the measured parameters, e.g. the displacement thickness or wall crossflow angle, was specified and the pressure distribution required to produce this development was calculated. It was then found that the calculated pressure distribution was only slightly different from the experimental, demonstrating again the sensitivity of the solution to the pressure field.

The lack of exact infinite-swept-wing conditions in the experiment may also be responsible for the observed differences between the calculations and the data. If a negative spanwise pressure gradient exists, this will produce an increased spanwise flow in the boundary layer and hence larger crossflow and earlier separation. The experimental data show no spanwise variation in pressure up to x = 1.22m, but a negative spanwise gradient is clearly seen further downstream. However, it is not known if this is strong enough to affect the flow significantly and account for the observed discrepancies.

Figures 1.5 and 1.6 show the velocity profiles at x = 0.92m and 1.12m. The profiles are plotted in streamline coordinates (note the difference in scales for U and W). At the first comparison station, x/c = 0.92, the wall crossflow angle was slightly underpredicted and this is reflected in the velocity profiles, i.e. somewhat higher streamwise and lower lateral velocity components. However, the computed profiles have the correct shapes, as would be expected from the close agreement in the integral parameters θ_{11}, H and wall shear stress.

At the second station, x = 1.12m, the deviations between the calculated and measured velocities are significant. The predicted streamwise velocity component is much too large and the crossflow component only about two-thirds of that measured. This is seen very clearly in the integral variables, like the momentum thickness, which at this position shows large deviations from the experimental values.

Figures 1.7 and 1.8 show a comparison between the calculated total shear and the experimentally obtained turbulent shear stresses. Of course, for a turbulent boundary layer there is very little difference between the total and turbulent shear because the turbulent stresses are at least two orders of magnitude larger than the molecular stresses, except for a region close to the wall which is of the order of 1/50 δ.

At x = 0.895m it is seen that the predicted shear stress distribution agrees qualitatively with the measurements. The computed peak value in $\overline{uv}$ is somewhat high, whereas the peak in $\overline{vw}$ is somewhat low. At x = 1.095m the predictions show neither qualitative nor quantitative agreement with the experiment. Because of the use of isotropic eddy viscosity in the predictions, the ratio of streamwise and lateral turbulent shear stresses is proportional to the ratio of the normal gradients of streamwise and lateral velocities. Since the lateral velocity component is almost an order of magnitude smaller than the streamwise component, $\overline{vw}$ is also small. However, the measurements indicate that the two components of the shear stress vector are of comparable magnitude. This is in fact one of the major results of the experiment, indicating a substantial difference between the directions of the turbulent stresses and the rates of strain. Fannelop and Humphreys (1974) have presented calculations using a non-isotropic eddy-viscosity model and

obtained some improvement in the predictions, but the lack of non-isotropy was introduced by a simple constant factor. This factor does not seem to be universal and therefore no attempt has been made to include it in the present calculations.

2. Boundary Layer with a Sudden Transverse Strain, LOHM73

2.1 Description of the problem. This is again a quasi two-dimensional problem in the sense that the flow is invariant in one direction. Th geometry consists of a circular cylinder, the forward part of which stationary and the rear rotates about the axis at a constant angul velocity, Ω. The external flow direction is along the cylinder axis so th the boundary layer is initially axisymmetric. On the rotating part of t wall, the boundary condition is suddenly changed from zero tangential velocity to ΩR, where R is the radius of the cylinder.

The measurements are due to Lohmann (1973), and the test case chosen for the workshop corresponds to

$$\frac{R}{L} = 5.277$$

$$\frac{W_0}{U_\infty} = \frac{\Omega R}{U_\infty} = 1.411 \quad \text{for } x/L > 0$$

(see figure 2.1), where U_∞ is the freestream velocity, W_0 is the tangential surface velocity due to rotation and L is the reference length.

In a fixed cylindrical coordinate system, the boundary-layer equations are

$$\frac{\partial U}{\partial x} + \frac{\partial V}{\partial y} + \frac{1}{r}\frac{\partial W}{\partial \theta} = 0$$

$$U\frac{\partial U}{\partial x} + V\frac{\partial U}{\partial y} = \frac{1}{\rho}\frac{\partial \tau_{xy}}{\partial y} \qquad (2.1)$$

$$U\frac{\partial W}{\partial x} + V\frac{\partial W}{\partial y} = \frac{1}{\rho}\frac{\partial \tau_{xz}}{\partial y}$$

and the boundary conditions at the edge of the boundary layer ($y = \delta$) and at the surface ($y = 0$) are, respectively,

$$U = U_\infty, \qquad W = 0$$

$$U = 0, \qquad W = W_0 = \Omega R$$

This case was also calculated using the infinite-yawed-cylinder flow option in the method. The measured initial velocity profile (at x/L = 0.5) was used to start the solution. However, since the data did not contain points close to the surface, the law of the wall was used to complete the profile. The solution marched along the axis of the cylinder.

The number of grid points across the boundary layer varied from 25 to 28 and a total of 56 streamwise steps were used to traverse the required calculation domain.

2.2 Results. The calculations are compared with the experimental data in figures 2.2 through 2.4. In general, the agreement is seen to be satisfactory in all respects except in the details of the Reynolds stresses (figure 2.4). The stress in the axial direction ($\overline{uv}$) is over-estimated while that in the tangential direction ($\overline{vw}$) is under-estimated. Once again, this may be attributed to the assumption of an isotropic eddy viscosity. However, the rather good agreement in the velocity profiles inspite of the substantial differences in the Reynolds stresses is perplexing since it would imply that incorporation of a non-isotropic model, to improve the agreement in the Reynolds stresses, may lead to poorer agreement in the mean velocity field. An alternative conclusion is that the flow is not particularly sensitive to the turbulence model.

An attempt was also made to study the direct influence of rotation on the turbulence by repeating the calculations with the eddy viscosity increased by

$$\frac{\nu_T}{\nu_{To}} = (1 - \beta R_i)^2 \qquad (2.2)$$

where $\beta = 4.5$, ν_{To} is the eddy viscosity in the absence of rotation and R_i is the Richardson number defined by

$$R_i = \frac{\frac{2W}{r}\frac{\partial}{\partial r}(Wr)}{\left[\left(\frac{\partial U}{\partial r}\right)^2 + \left(\frac{\partial W}{\partial r}\right)^2\right]} \qquad (2.3)$$

The results, which were also presented at the workshop, did not indicate any significant improvement in the prediction of the Reynolds stresses since both components were increased by about 20% in the inner region. The influence on the integral parameters and the mean velocity profiles was too small to draw any definite conclusions on the desirability of such a correction.

3. Boundary Layer Ahead of an Obstacle, DEFE77

3.1 Description of the problem. This test case is a true three-dimensional problem because the three velocity components depend on all three space coordinates. The experiment was performed by Dechow and Felsch (1977) and is similar to that first considered by Hornung and Joubert (1963) and later by East and Hoxey (1969) and Krogstad (1979). However, only Dechow and Felsch measured the Reynolds stress tensor. The geometry consists of the junction of a wing type body and a flat plate (figure 3.1) and the interest lies in predicting the development of the boundary layer on the flat surface upstream of the junction. The boundary layer finally separates and leads to a horse-shoe vortex in the corner. The three-dimensionality is generated primarily by the pressure field as the pressure builds up in front of the stagnation line. With this sudden increase in pressure ahead of the body, the pressure gradient terms dominate the momentum equations and therefore the velocity field changes drastically over a short distance, of the order of one boundary layer thickness upstream of the central part of the separation line.

The test case was specified by the velocity and shear-stress profiles along an initial line ($x = 0$) and a table of the pressure coefficients measured at the wall. Because the problem is fully three-dimensional it is necessary to determine the velocity field outside the boundary layer from the experimental pressure distribution. However, this is not a trivial task since it requires the solution of Euler's equations. Since such a program was not available, it was decided to follow Tai (1981), who suggested a simple method for tracing streamlines from a two-dimensional table of pressure coefficients. For documentation of this calculation, see Krogstad (1982).

Once the streamlines are known, the two external velocity components are easily obtained. Since the boundary-layer calculations were required only up to the first point of separation, Cartesian coordinates were used. In this case the method of Tai reduces to solving the very simple equation

$$\frac{\partial \gamma}{\partial x} = \frac{\frac{\partial C_p}{\partial x} \tan\gamma - \frac{\partial C_p}{\partial z}}{2(1 - C_p)} \qquad (3.1)$$

γ being the angle between the streamline and the x-axis.

The measured pressure coefficients were spline-fitted, both along x and z, and the gradients of C_p were found by a third-order interpolation scheme. After specifying the initial streamline direction (given in the input data) and the starting coordinates of the streamlines to be traced, equation (3.1) was solved using a fourth-order accurate Runge-Kutta scheme. Simultaneously, the velocity components along the streamlines were calculated and transformed to the Cartesian coordinate system used to solve the boundary-layer equations by a new series of spline fittings. The streamlines thus obtained are shown in figure 3.2 and coincide exactly with the streamlines traced by Dechow and Felsch.

In the boundary-layer calculations, a total of 12 non-uniformly spaced lateral grid lines and 69 streamwise steps were taken. 33 grid points perpendicular to the surface were used. Along the line of symmetry the proper set of equations were solved and used as boundary conditions for the fully 3D calculation along the other lines.

3.2 Results. Figure 3.3 shows the variation of the skin friction coefficient as function of the streamwise distance x/L for different z/L (see figure 3.2 for the location of the lines). The computations were started using the same two-dimensional profile for all lines as the experimental initial profiles showed very little variation. As is to be expected, the skin friction coefficient decreases fastest along the line of symmetry where the streamwise adverse pressure gradient is strongest. Both the centerline skin friction distribution and the distribution along z/L = 0.06 seem to indicate a development towards separation at around x/L = 0.85. However, the flow

appears to recover rapidly beyond x/L = 0.87. (Separation along z/L = 0 was finally predicted around x/L = 1.01). From the limited experimental information available, it was known that separation occurred at the centerline around x/L = 0.89. An examination of the wall pressure measurements indicated a region of constant pressure from x/L = 0.87 to x/L = 0.96 (see figure 3.4) which, when spline-fitted, produced a favorable pressure gradient and therefore a recovery in the boundary-layer calculations. This region of constant pressure in the data may be due to the viscous-inviscid interaction in the neighborhood of separation. The discontinuity in the pressure coefficient was smoothed as shown in figure 3.4 and the calculations were repeated. The distribution of skin friction coefficient using the modified pressure distribution is shown in figure 3.5 and separation is predicted at x/L = 0.89 at the line of symmetry, in agreement with experimental observations. Figures 3.6 and 3.7 show comparisons between the measured and computed development of the Reynolds number based on momentum thickness and the wall crossflow angle along the streamline starting at z/L = 0.14. The agreement is seen to be satisfactory. The rapid development in the three-dimensionality is also seen from the rapid increase in the wall crossflow angle upstream of the separation point. (For this streamline, separation occurs at x/L ≈ 0.92). At x/L = 0.9 the boundary layer thickness is 0.07L, and therefore the crossflow angle is tripled over about two boundary-layer thicknesses. This kind of rapid development is typical for flows with strong pressure gradients. Because there is such a strong coupling between the velocity terms and the pressure gradients in the momentum equations the rate of change of turbulent shear is less important. It is therefore found that the choice of turbulence model is not critical for such flows.

Only one velocity profile was available for comparison, namely the profile at x/L = 0.826 and z/L = 0.162 which is somewhat upstream of the separation line (measurement station 5). The velocity profile is shown in figure 3.8 and the agreement is again seen to be good.

Figure 3.9 shows the computed and measured shear stress profiles at measurement station 4 which is at x/L = 0.739 and z/L = 0.153. The agreement is seen to be good although the predicted magnitudes of both shear stresses are somewhat high.

4. Experiment of Muller and Krause, MUKR79

4.1 Description of the problem. This last case is also a true three-dimensional boundary-layer problem and was labelled "optional" by the organizers. The experiment was performed by Muller and Krause (1979). The geometry used is sketched in figure 4.1, and consists of a flat surface on which a boundary layer is allowed to develop. Streamwise and lateral pressure gradients are generated by means of a set of vanes. The initially two-dimensional boundary layer becomes three-dimensional and approaches separation.

Initial profiles and a two-dimensional map of pressure coefficients measured at the boundary-layer edge were given. Also the freestream flow angles were given so that the streamlines could be obtained directly by integration. However, instead of doing this, the streamline program mentioned earlier was used. In principle the two methods should produce identical results because the freestream flow angles must be compatible with the experimental pressure field.

This case was solved in a manner similar to the previous one. The solution was carried out in Cartesian coordinates by assuming plane of symmetry conditions along $z/L = 0$ (figure 4.2). However, pressure measurements were not available for the whole computational domain. Additional data were therefore "invented" where needed. This is considered legitimate provided the area where ficticious data was generated is outside the domain of dependence of the region over which the calculations are required. This domain is bounded by the initial line at which calculations are started, the wall streamline along the side boundary where inflow occurs (or the line of maximum crossflow angle if this is not the wall streamline) and the external streamline (or the line of minimum crossflow angle) along the side boundary for which outflow occurs). Figure 4.2 shows the streamline pattern obtained and also indicates the domain in which pressure data were available. After performing the boundary-layer computations, the domain of influence could be traced and it was confirmed that this area was confined to the region where the pressure data were given. Therefore the "invented" pressure field did not influence the solution in the area of interest.

The boundary-layer was computed along 11 uniformly-spaced lines of constant z/L from 0.0 to 0.5, using 37 points across the layer and 69 streamwise steps. Outputs were required at the four locations indicated by circles in figure 4.2.

4.2 Results. The first problem encountered in the calculations was that the boundary layer program would not accept the initial velocity profile generated using the experimental skin friction and momentum thickness, which were of the order of 3.1×10^{-3} and 2.5 mm, respectively. The computed skin friction coefficient oscillated markedly and reached quite large values. Because the development distance from the plate leading edge to the first measurement station was only 35 cm, the boundary-layer must have been tripped dramatically to produce such a thick boundary-layer over such a short distance ($\delta \simeq 5$ cm or $x \sim 7\delta$). Also the distance between the trip and the first measurement station is much too short for the boundary layer to recover from the tripping. Therefore, the initial integral data are believed to be of limited value in determining a standard starting profile. A new profile was generated by manipulating the skin friction coefficient and the momentum thickness to produce a profile that resembled the measured profile as close as possible. This profile is shown in figure 4.3. The corresponding skin friction coefficient is 3.2×10^{-3} and the momentum thickness is 3.0 mm. This profile was used all along the initial line.

The second problem was discovered when the integral data were plotted as functions of z/L at constant x/L. Figure 4.4 shows the distribution of the wall crossflow angle at x/L = 0.4. It is seen that the distribution shows a number of wiggles. The same was true for the other variables such as the skin friction coefficient, shape factor and momentum thickness. Although the amplitude of the oscillation is only about 15% the same trend was found at all values of x/L. At first it was believed that this was due to numerical errors because the lateral step size in the streamline program was not constant. However, recalculating the flow with another coordinate grid of constant spacing caused similar wiggles.

Upon inspecting the pressure field it was found that although the experimental pressure field appears quite smooth both the streamwise and

lateral pressure gradients show considerable oscillations. Figure 4.5 shows the pressure gradients at x/L = 0.4 and the wiggles in $\partial C_p/\partial z$ are easily correlated with those in the wall crossflow angle. Of course, the wiggles will depend on the location of the lines along which the calculations are performed. This demonstrates very clearly the difficulties involved, and the care that must be taken, in using experimental pressure fields as input data. Unfortunately, smoothing of the pressure field is very difficult and may be very dangerous in a two-dimensional data table, and therefore was not attempted.

Figure 4.6 shows the streamwise distribution of the skin friction coefficient along z/L = 0.5. The agreement is seen to be quite good although the measurements indicate that the computations could have been started with an even higher initial value. Figures 4.7 and 4.8 show the corresponding distributions of the Reynolds number based on the momentum thickness and the wall crossflow angle, respectively. The general behavior is correctly predicted although systematic differences are apparent in both quantities. Figure 4.9 shows a comparison between the measured and computed velocity profiles at x/L = 0.6 and z/L = 0.5 for which the experimental wall crossflow angle is about 25°. The agreement is seen to be quite good, both in U/U_e and W/U_e, inspite of the various difficulties noted earlier.

Comparisons were also made for the shear-stress profiles at the above station. However, these showed very large discrepancies. This was also the case for the calculations made by the other participants in the Berlin Workshop and strong doubts were expressed about the measurements, at least as interpreted by the organizers. Consequently, we shall not discuss these until this issue is resolved.

IV. CONCLUSIONS

The four calculations presented here illustrate the general performance of the method of Chang and Patel (1975). They also point out some of the

difficulties associated with making such calculations and drawing definitive conclusions relative to the specific ingredients of the method, such as the numerics and the turbulence model. The comparisons with the data and with the results of the other methods presented at the workshop suggest that the present method performs just as well as any of the methods available at the present time. A comparative evaluation of the methods will appear in the workshop proceedings.

On the basis of the calculations presented here, it appears that a simple eddy-viscosity model is successful in predicting the most important features of the four test cases, provided there are no thick boundary-layer effects and viscous-inviscid interactions. Unfortunately, three of the four test cases, namely BEEL72, DEFE77 and MUKR79, contain such regions. The failure of all methods, which include integral as well as differential methods, in the first case beyond $x = 1.05$ is well known and, as discussed in the text, may be due to viscous-inviscid interation, lack of spanwise invariance, or both, rather than the turbulence model. In the other two cases, the zones of three-dimensional flow are relatively short, in terms of local boundary layer thickness, and the flows progress rapidly towards searation. The last case also indicates the importance of specifying the pressure gradients, in place of the pressure field, in future workshops since the results are influenced by the uncertainties in the determination of the gradients. Finally, the two fully three-dimensional cases, namely DEFE77 and MUKR79, are pressure-driven flows and therefore are not particularly suitable for the evaluation of turbulence models.

V. ACKNOWLEDGEMENTS

The work reported here was supported, in part, by the General Hydromechanics Research Program of the Naval Sea Systems Command, Department of the Navy, technically administered by the David W. Taylor Naval Ship Research and Development Center under Contract N00014-82-K0200.

VI. REFERENCES

van den Berg, B. and Elsenaar, A. (1972) "Measurements in a three-dimensional incompressible turbulent boundary layer under infinite swept wing conditions", NLR TR 72092 U.

Cebeci, T. and Bradshaw, P. (1977) "Momentum Transfer in Boundary Layers", McGraw Hill.

Chang, K.C. and Patel, V.C. (1975) "Calculation of three-dimensional boundary layers on ship forms", IIHR Report 178.

Choi, D.H. (1978) "Three-Dimensional Boundary Layers on Bodies of Revolution at Incidence", Ph.D. Thesis, The University of Iowa.

Dechow, R. and Felsch, K.O. (1977) "Measurements of the mean velocity and of the Reynolds stress tensor in a three-dimensional turbulent boundary layer induced by a cylinder standing on a flat wall", Proc. 1st Symp. Turbulent Shear Flows, Penn State University, Pa.

East, L.F. (1975) "Computation of three-dimensional turbulent boundary layers, Euromech 60, Trondheim 1975", FFA TN AE-1211.

East, L.F. and Hoxey, R. (1969) "Low speed three-dimensional turbulent boundary layer data", Royal Aircraft Establishment TR 69041 and TR 69137.

Elsenaar, A. and Boelsma, S.H. (1974) "Measurement of the Reynolds stress tensor in a three-dimensional turbulent boundary layer under infinite swept wing conditions," NLR TR 74095 U.

Fannelop, T.K. and Humphreys, D.A. (1974) "A simple finite-difference method for solving the three-dimensional turbulent boundary layer equations", Proc. 12th Aerospace Sciences Meeting, AIAA.

Fannelop, T.K. and Krogstad P.A. (1975) "Three-dimensional turbulent boundary layers in external flows: A Report on Euromech 60", J. Fluid Mech., Vol. 71.

Humphreys, D.A. (1979) "Comparison of boundary layer calculations for a wing: the May 1978 Stockholm Workshop test case" FFA TN AE-1522.

Humphreys, D.A. (1981) "1 April 1982 Berlin Workshop; Documentation to accompany the test case data" FFA Report.

Hornung, H.G. and Joubert, P.N. (1963) "The mean velocity profile in three-dimensional turbulent boundary layers", J. Fluid Mech., Vol. 15, p. 368.

Kline, S.J., Morkovin, M.V., Sovran, G. and Cockrell, D.J. (1968) "Computation of Turbulent Boundary Layers", Proc. AFOSR-IFP-Stanford Conference.

Krogstad, P.A. (1979) "Investigation of a three-dimensional turbulent boundary layer driven by simple two dimensional potential flow", Ph.D. Thesis, Norweigan Institute of Technology.

Krogstad, P.A. (1982) "A users manual for the IIHR streamline program", IIHR LD Report, (to be published).

Larsson, L. (1981) 'SSPA - ITTC Workshop on Ship Boundary Layers, 1980" SSPA Report 90.

Lindhout, J.P.F., van den Berg, B. and Elsenaar, A. (1981) "Comparison of boundary layer calculations for the root section of a wing", NLR MP 80028 U.

Lohmann, R.P. (1973) "The response of a developed turbulent boundary layer to local transverse surface motion", Ph.D. Thesis, University of Connecticut. Also, ASME, J. Fluids Eng., Vol. 98, p. 354, 1976.

Muller, U. and Krause, E. (1979) "Measurements of mean velocities and Reynolds stress in an incompressible three-dimensional turbulent boundary layer", Proc. 2nd Symp. Turbulent shear flows, Imperial College, London.

Patel, V.C. and Baek, J.H. (1982) "Calculation of three-dimensional boundary layers on bodies at incidence", 7th U.S. Air Force and Federal Republic of Germany Data Exchange Agreement Meeting, USA-BRL, Aberdeen Proving Grounds, Maryland.

Patel, V.C. and Choi, D.H. (1980) "Calculation of three-dimensional laminar and turbulent boundary layers on bodies of revolution at incidence", Turbulent Shear Flows 2, Springer-Verlag, p. 199.

Tai, T.C. (1981) "Determination of three-dimensional flow separation by a streamline method", AIAA Journal, Vol. 19, p. 1264.

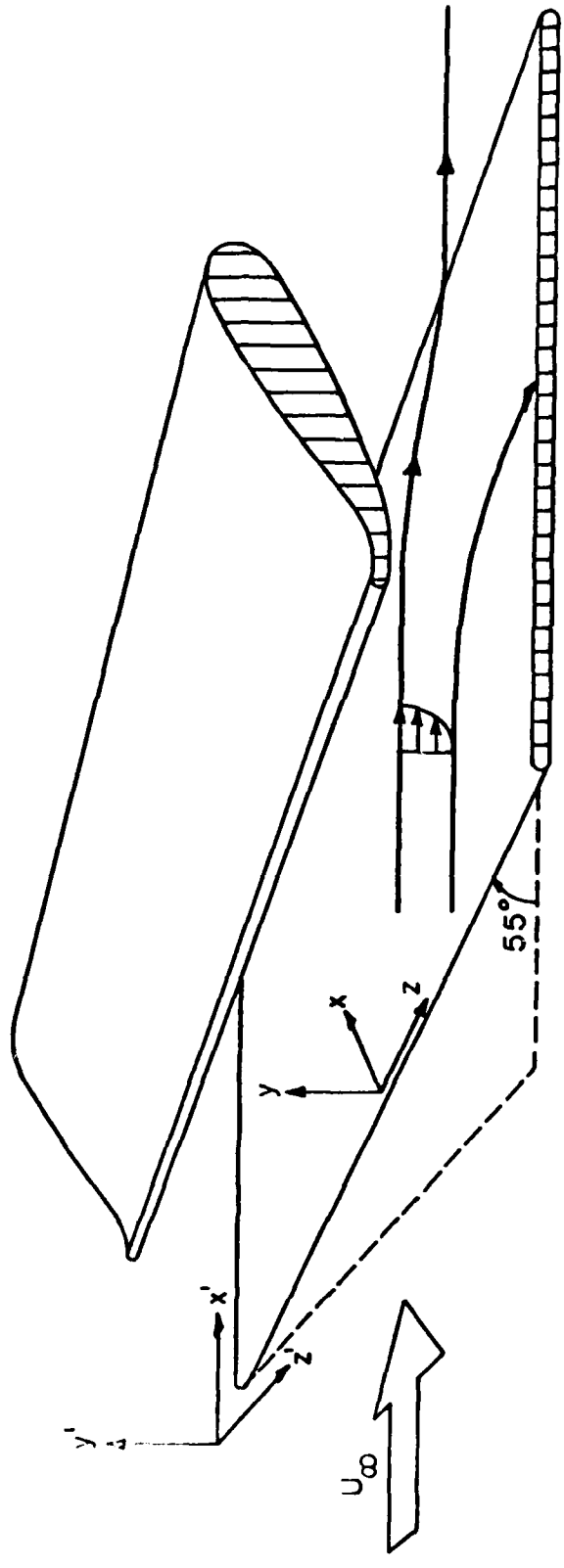

FIG. 1.1 GEOMETRY IN BEEL72 TEST CASE

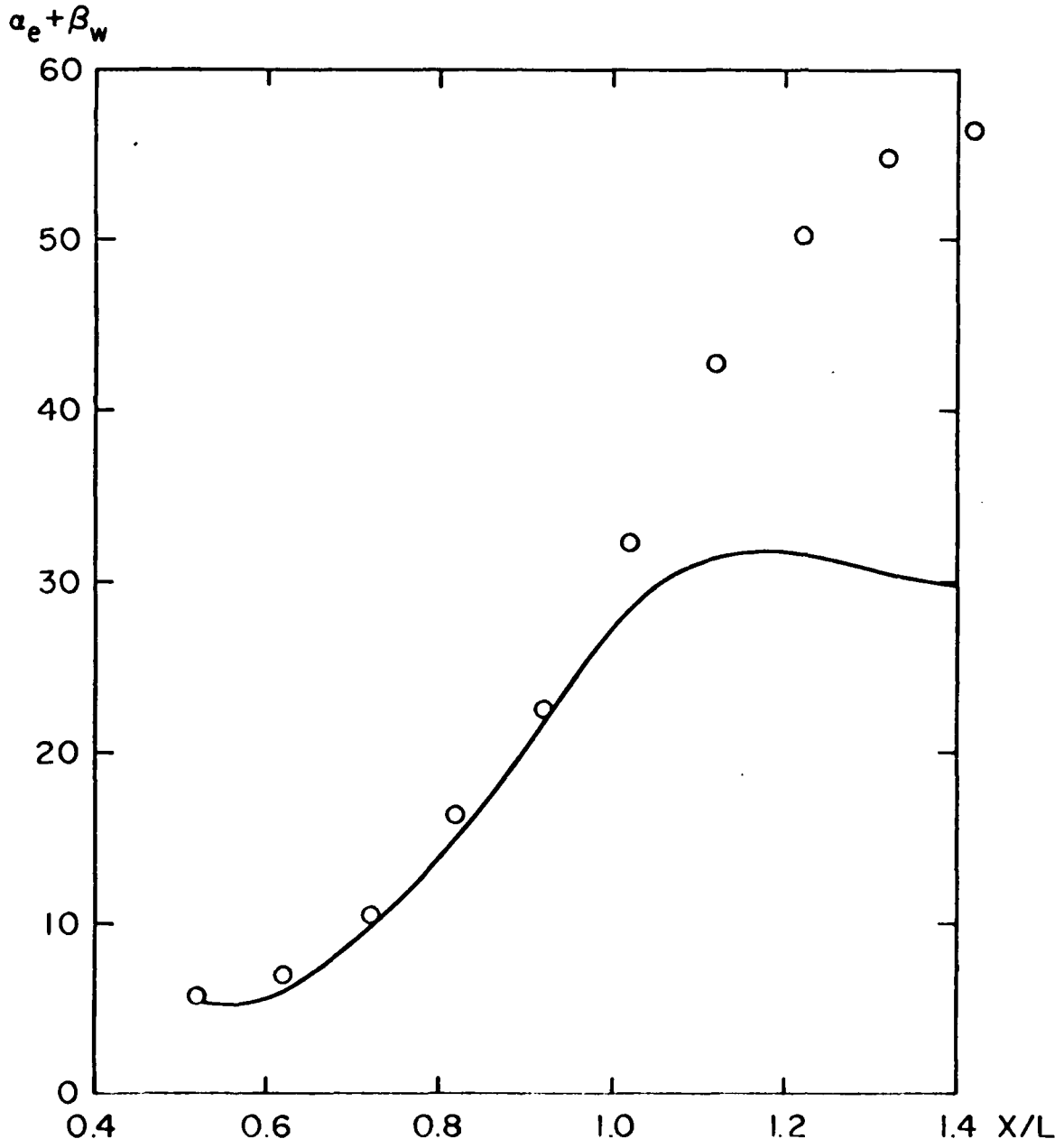

FIG. 1.2 ANGLE BETWEEN WALL STREAMLINE AND TUNNEL AXIS, BEEL72

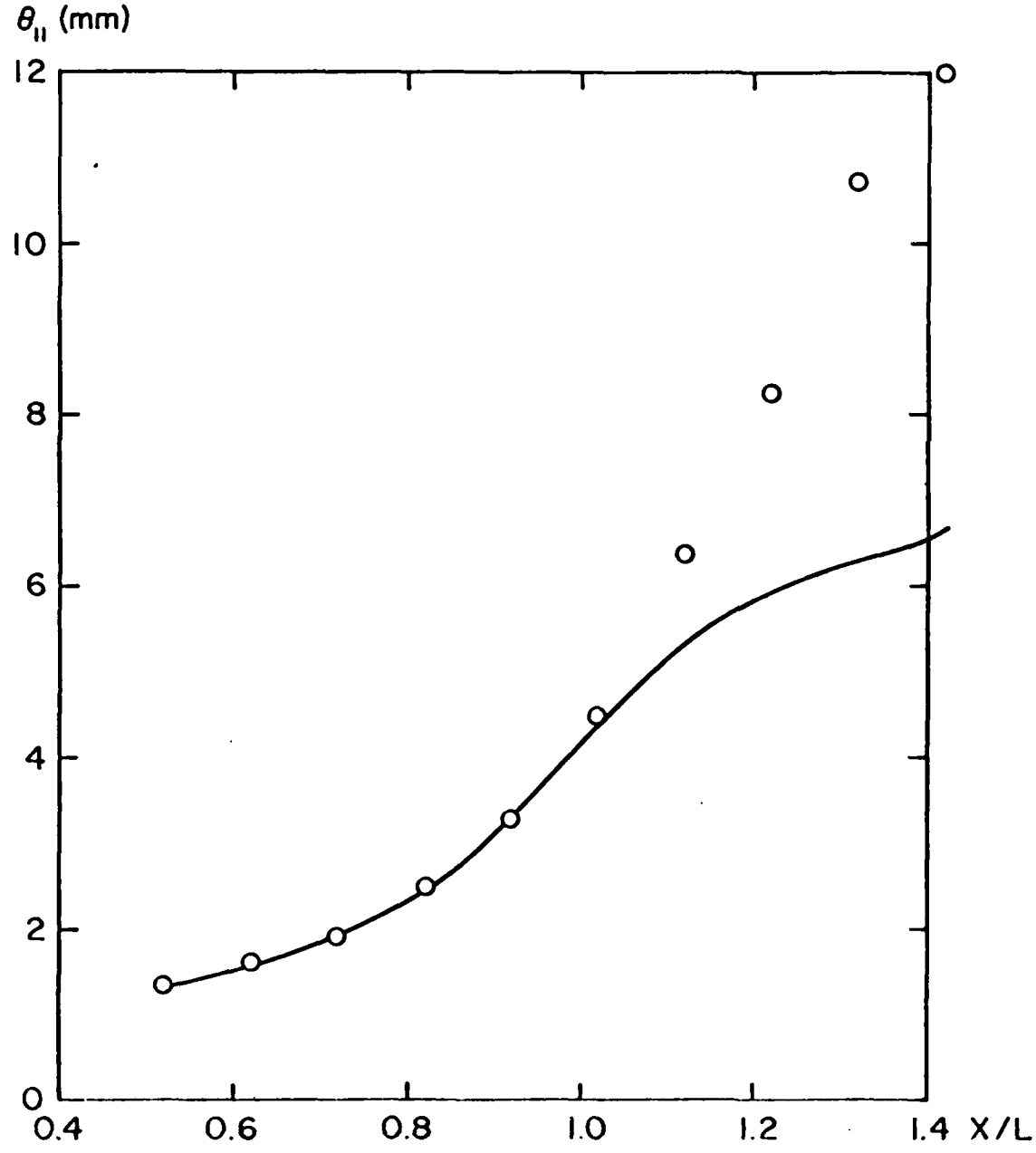

FIG. 1.3 MOMENTUM THICKNESS, BEEL72

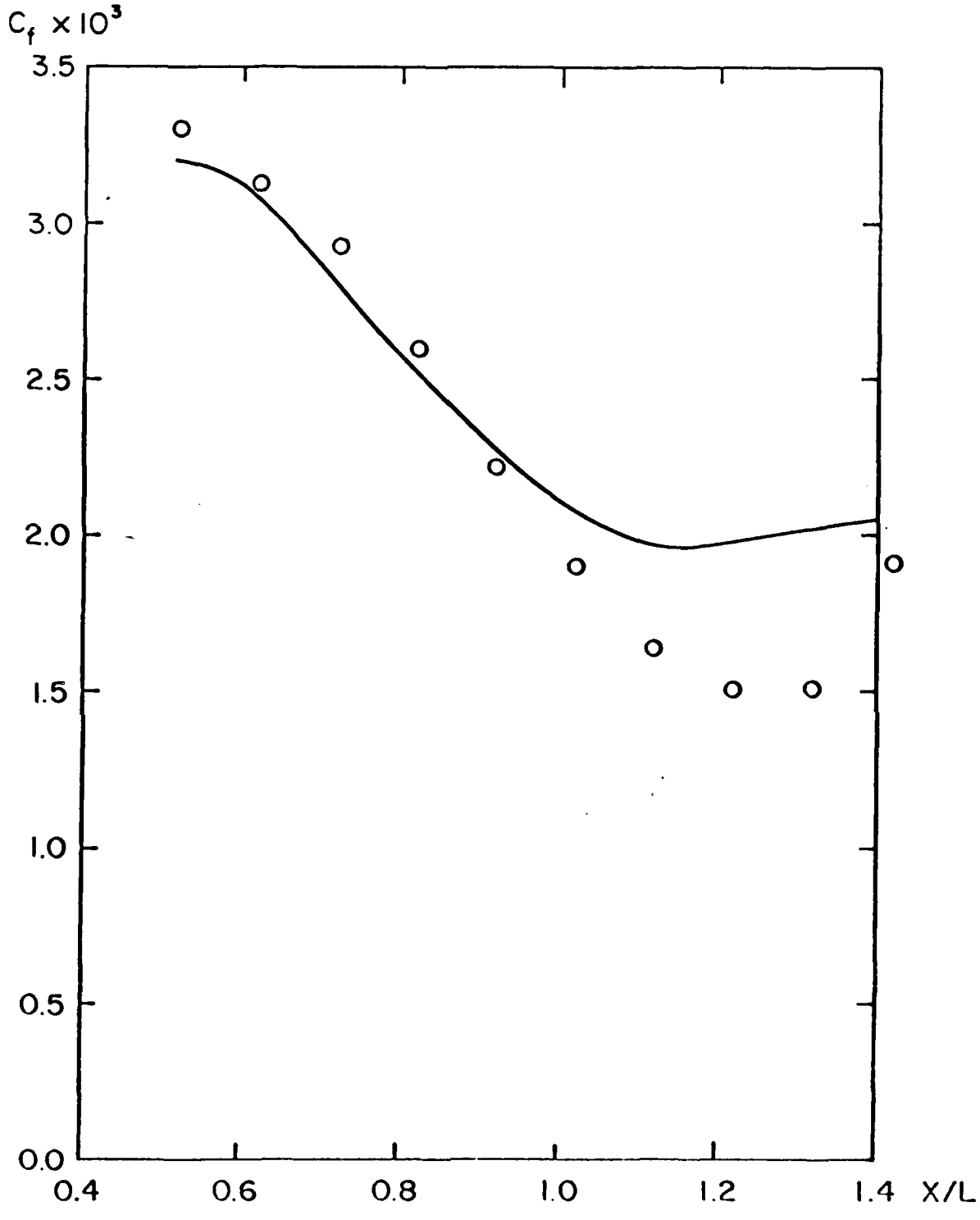

FIG. 1.4 SKIN-FRICTION COEFFICIENT, BEEL72

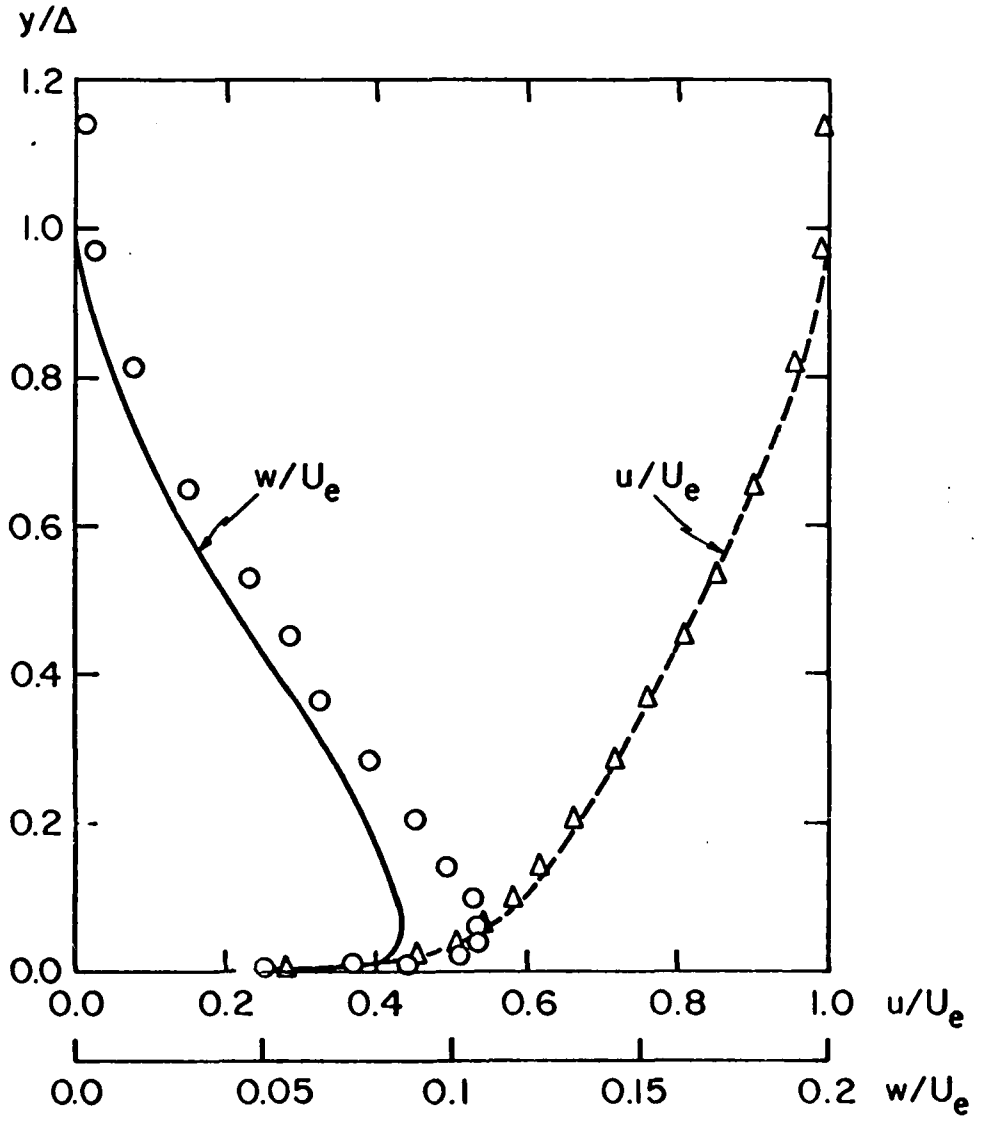

FIG. 1.5 VELOCITY PROFILES AT x/L = 0.92, BEEL72

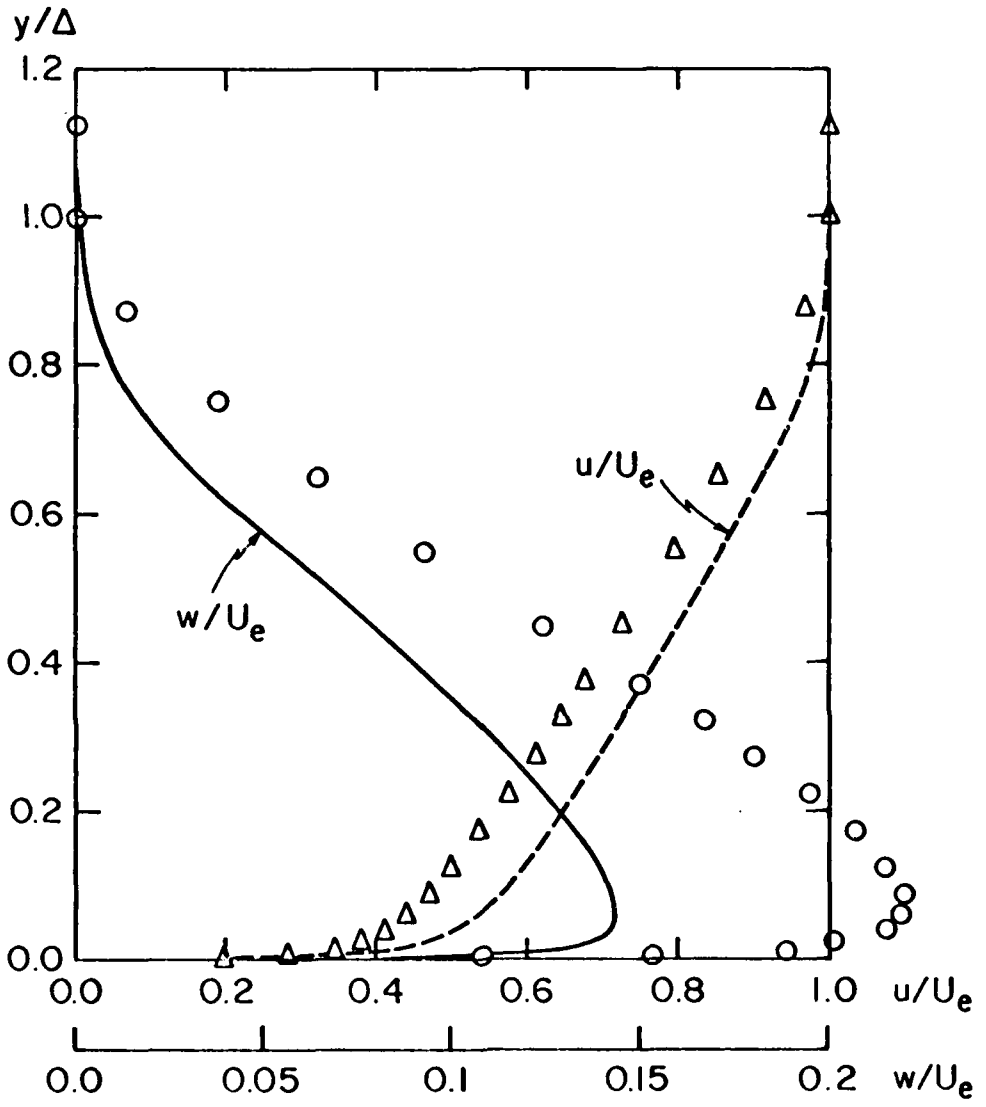

FIG. 1.6 VELOCITY PROFILES AT x/L = 1.12, BEEL72

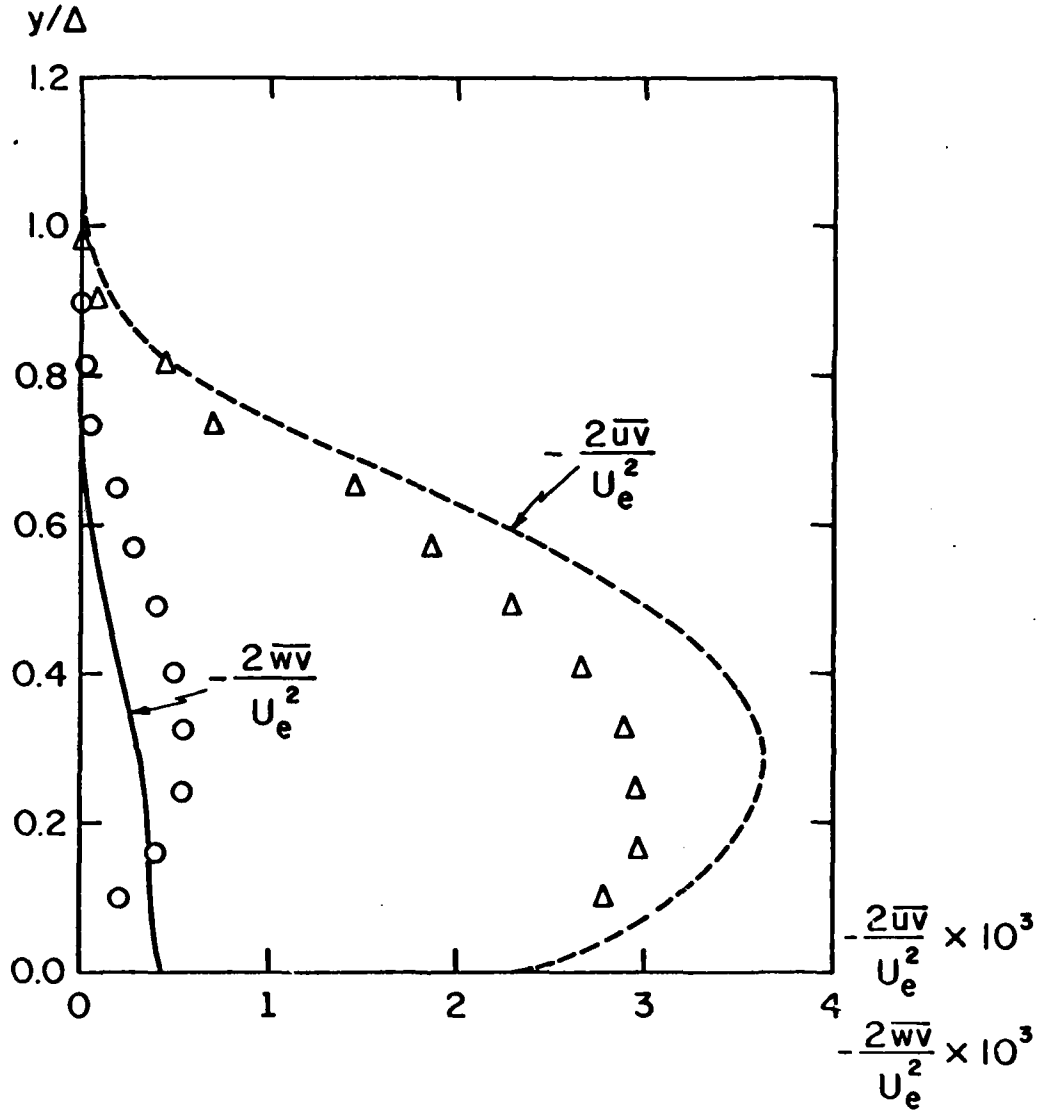

FIG. 1.7 SHEAR-STRESS PROFILES AT x/L = 0.895, BEEL72

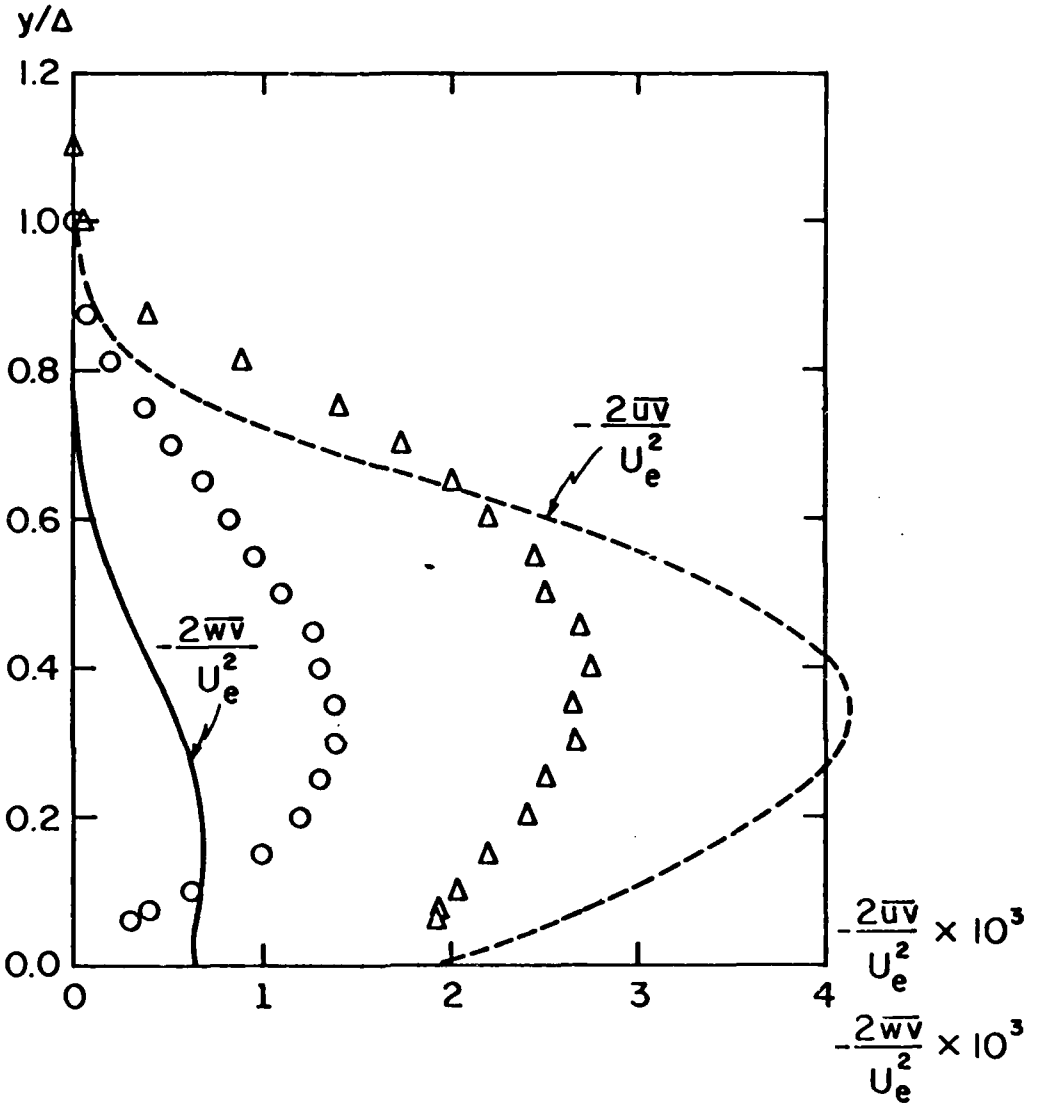

FIG. 1.8 SHEAR-STRESS PROFILES AT x/L = 1.095, BEEL72

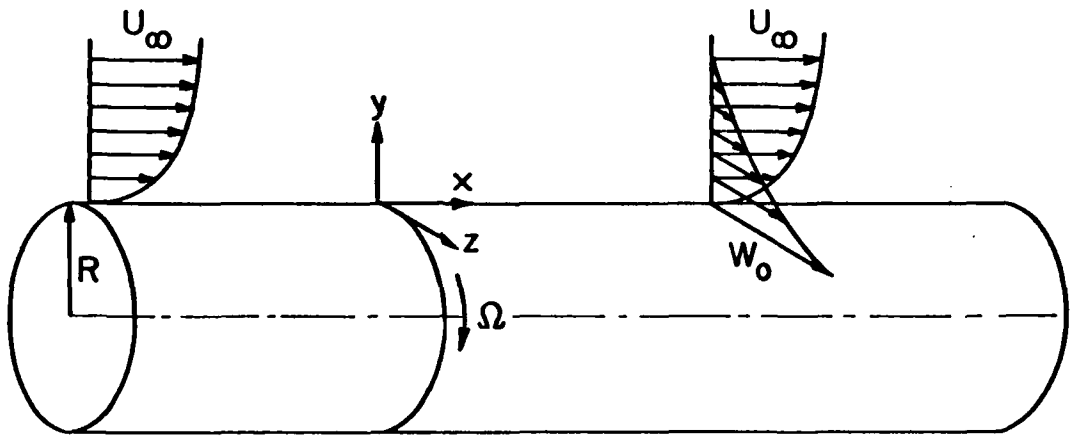

FIG. 2.1 GEOMETRY IN LOHM73 TEST CASE

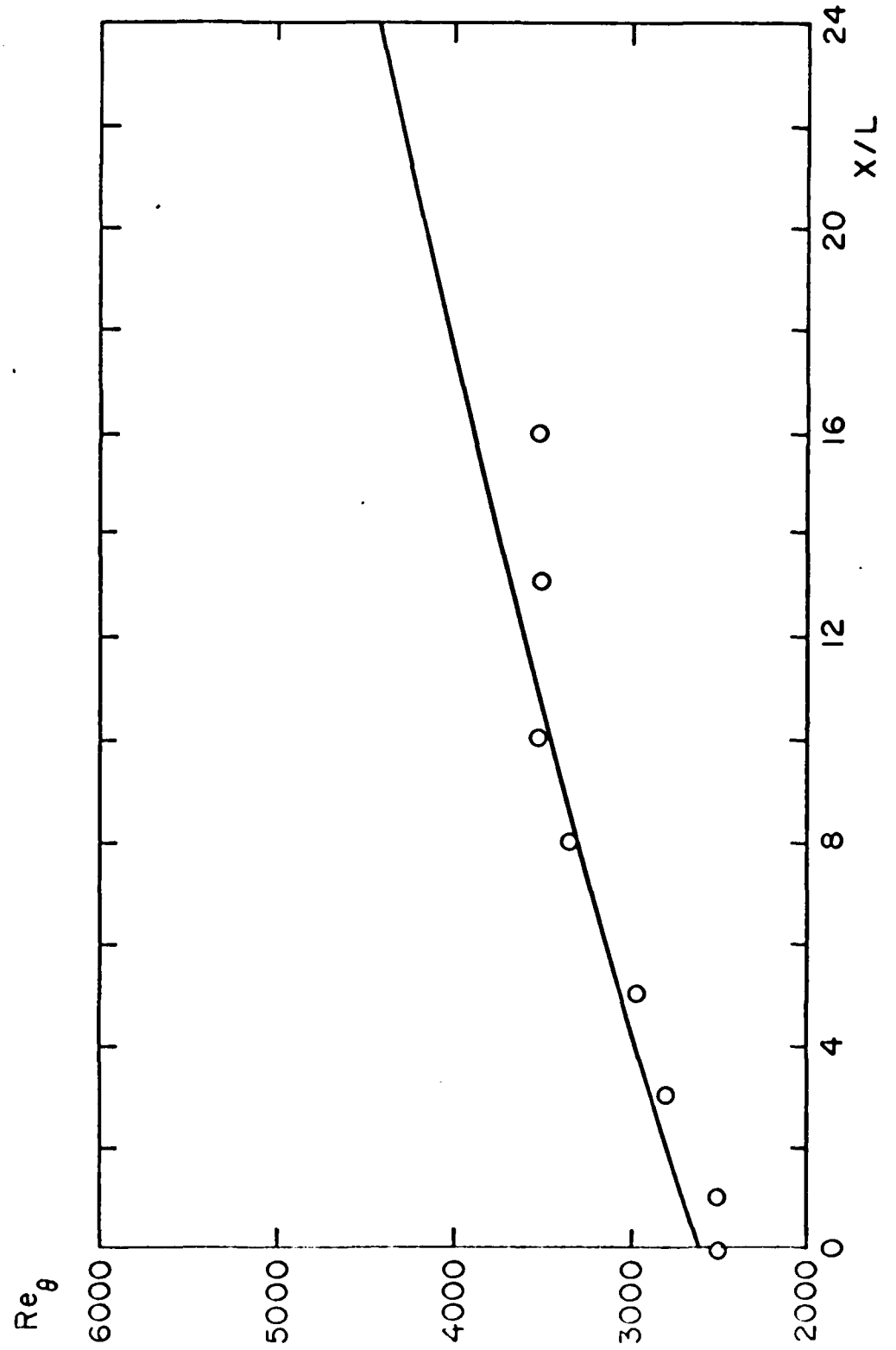

FIG. 2.2 MOMENTUM-THICKNESS REYNOLDS NUMBER, LOHM73

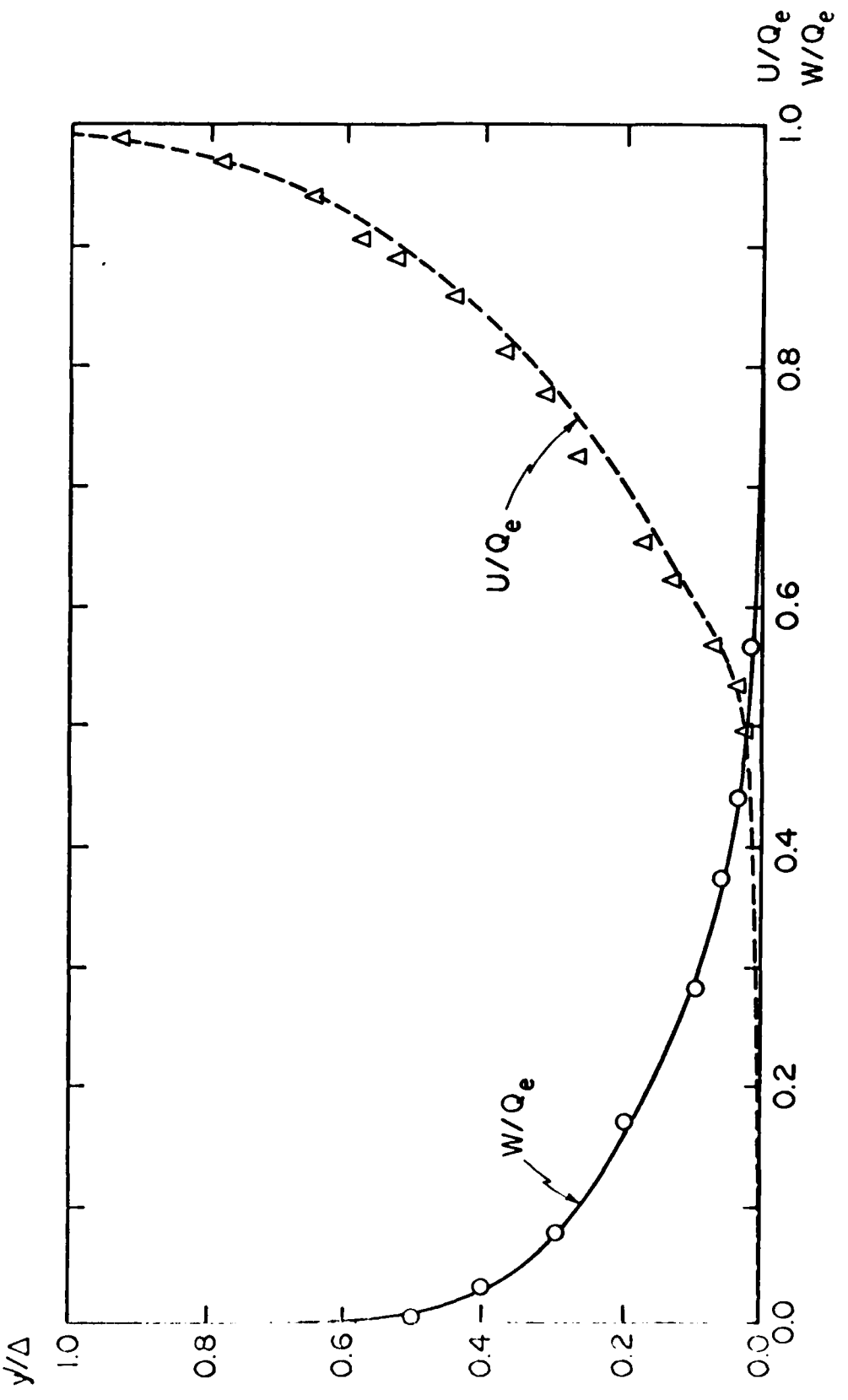

FIG. 2.3 VELOCITY PROFILES AT x/L = 8, LOHM73

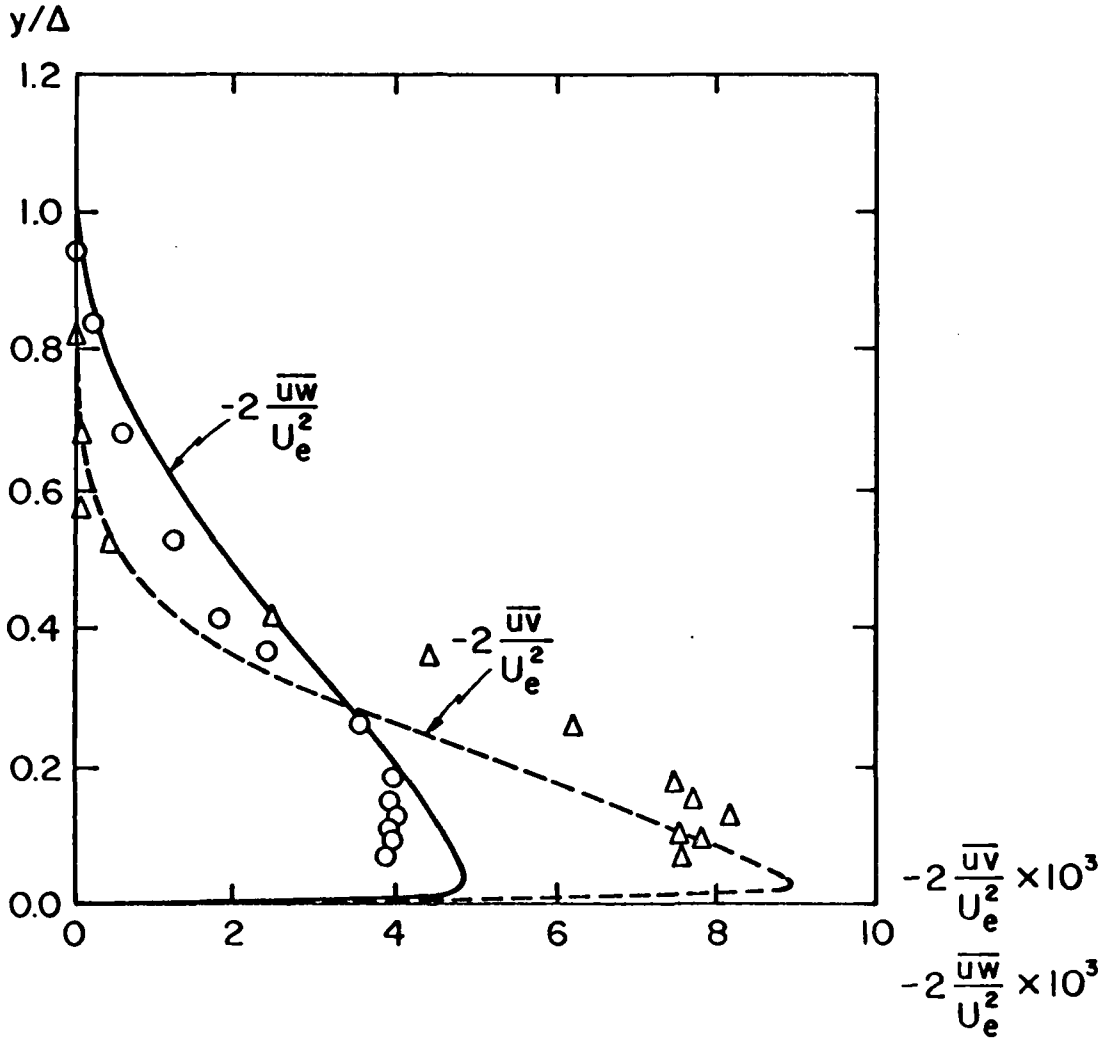

FIG. 2.4 REYNOLDS-STRESS PROFILES AT x/L = 8, LOHM73

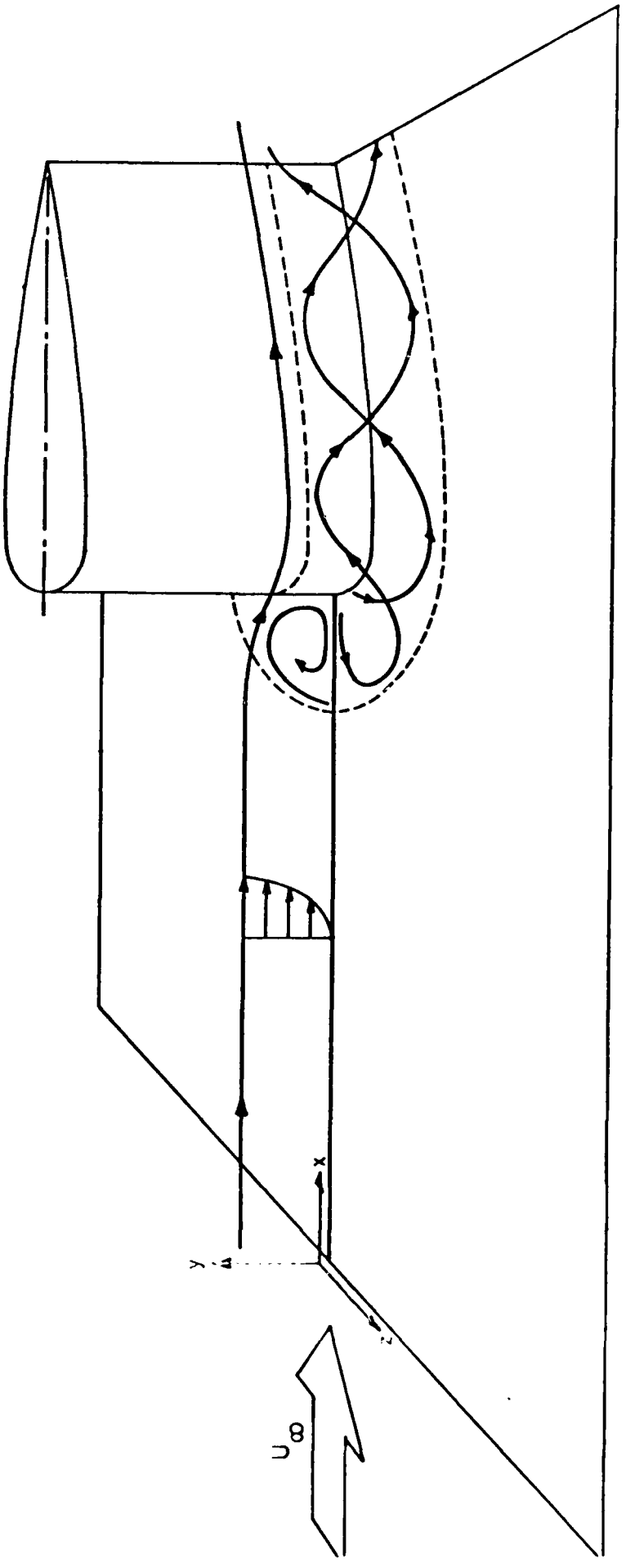

FIG. 3.1 GEOMETRY OF DEFE77 TEST CASE

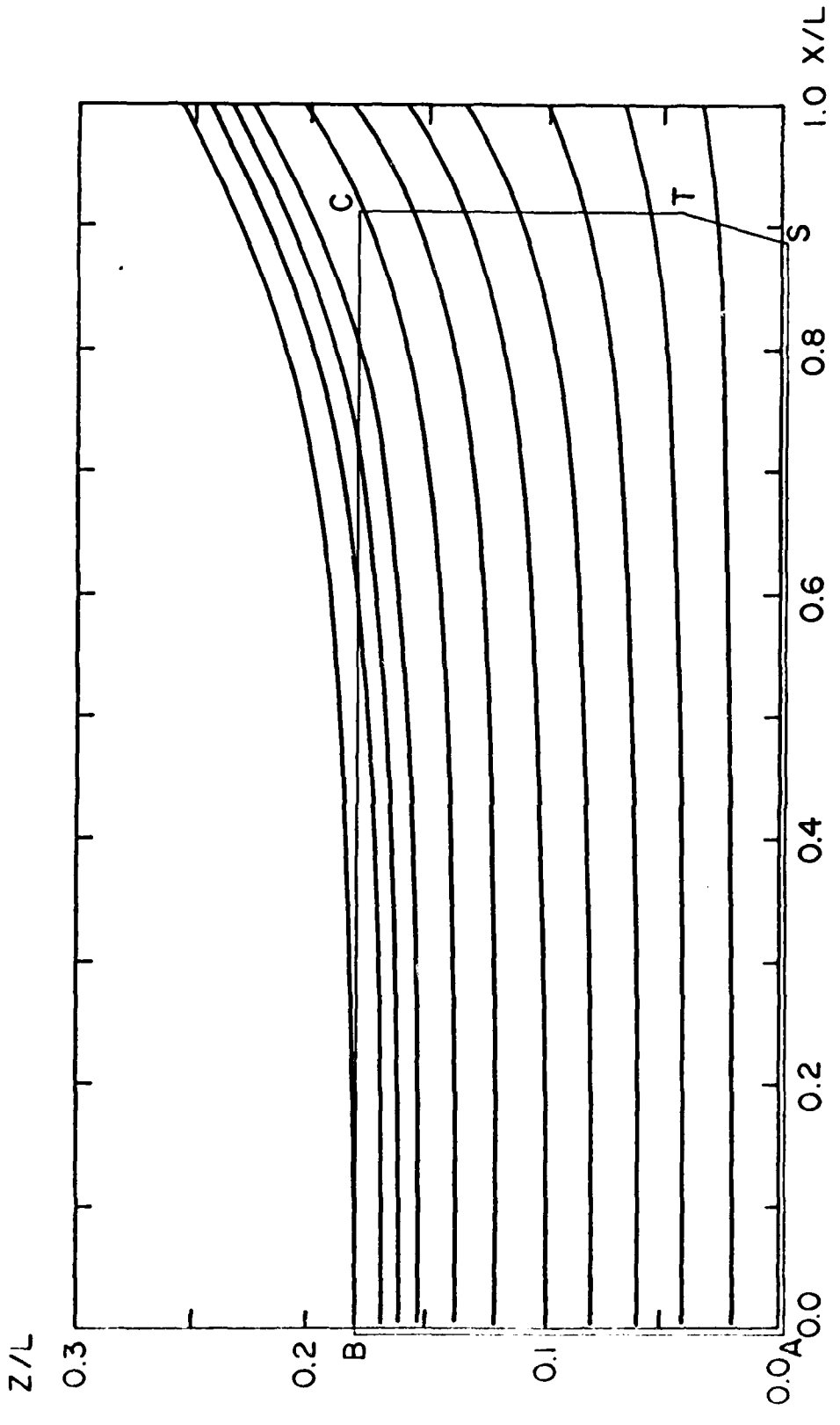

FIG. 3.2 EXTERNAL STREAMLINES IN DEFE77. AB: INITIAL LINE, AS: SYMMETRY LINE, ST: CALCULATED SEPARATION LINE

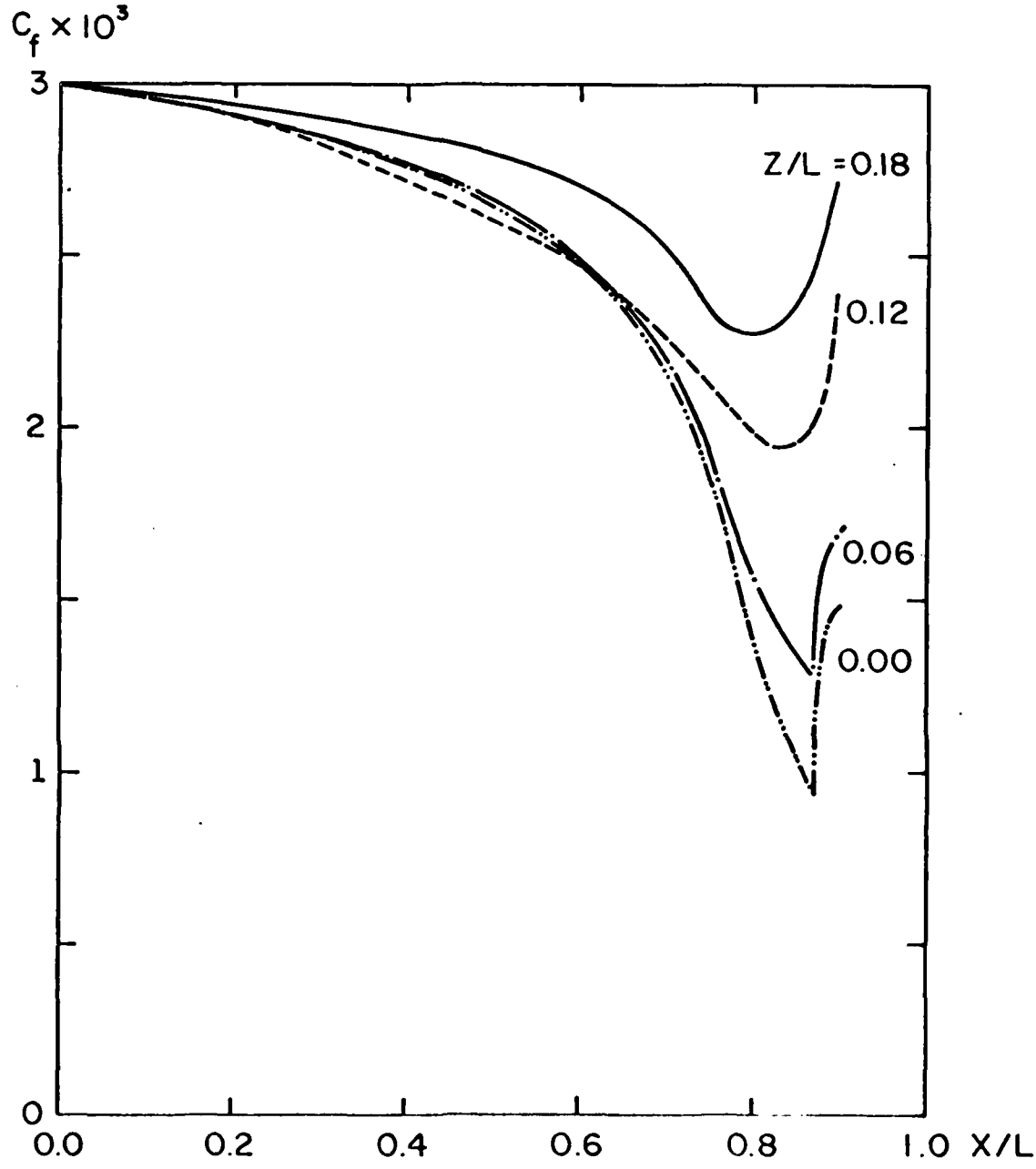

FIG. 3.3 SKIN-FRICTION COEFFICIENT WITH PRESCRIBED PRESSURE FIELD, DEFE77

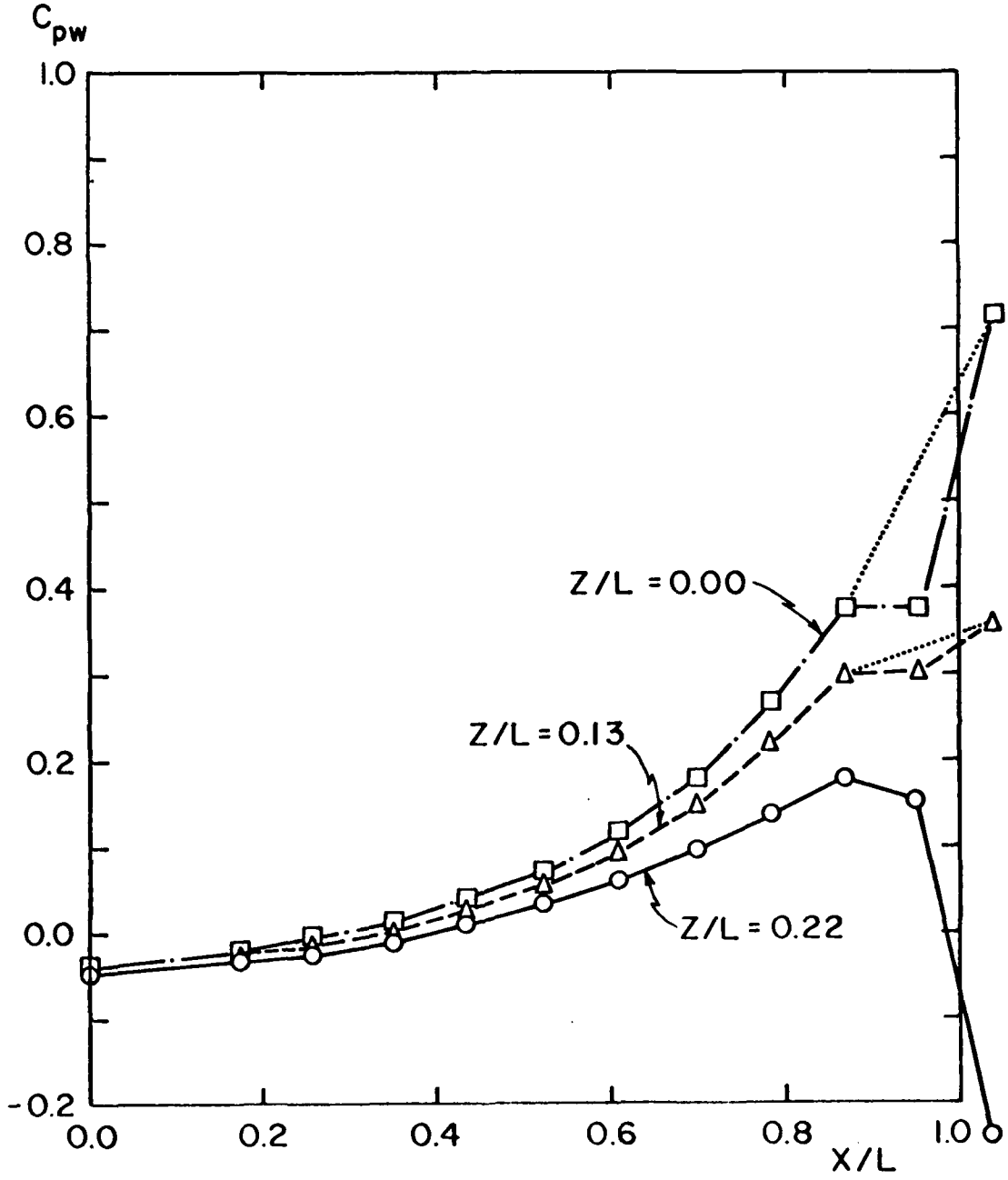

FIG. 3.4 WALL PRESSURE DISTRIBUTION IN DEFE77

○ △ □ MEASURED

..... MODIFICATION

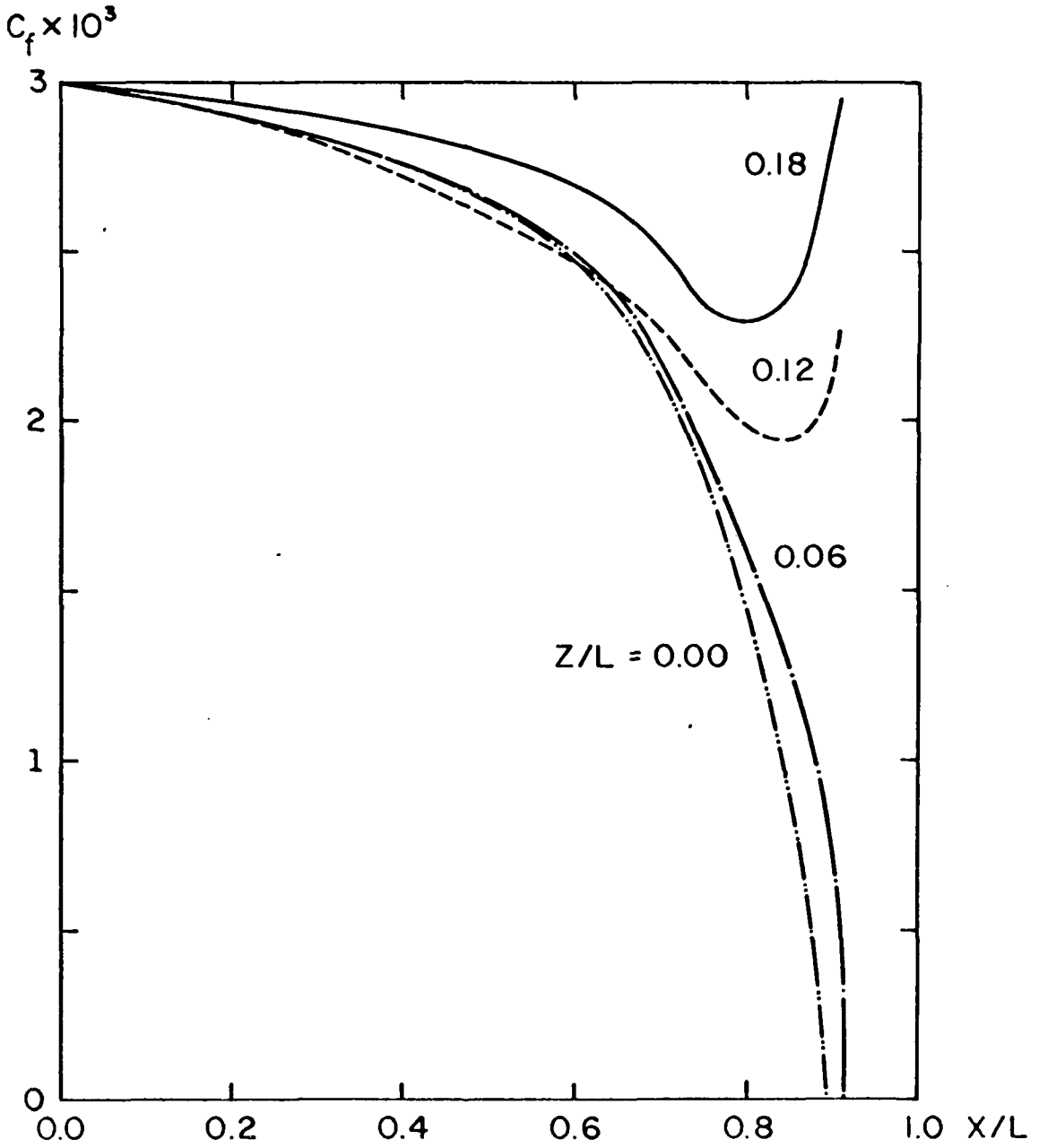

FIG. 3.5 SKIN-FRICTION COEFFICIENT WITH MODIFIED PRESSURE FIELD, DEFE77

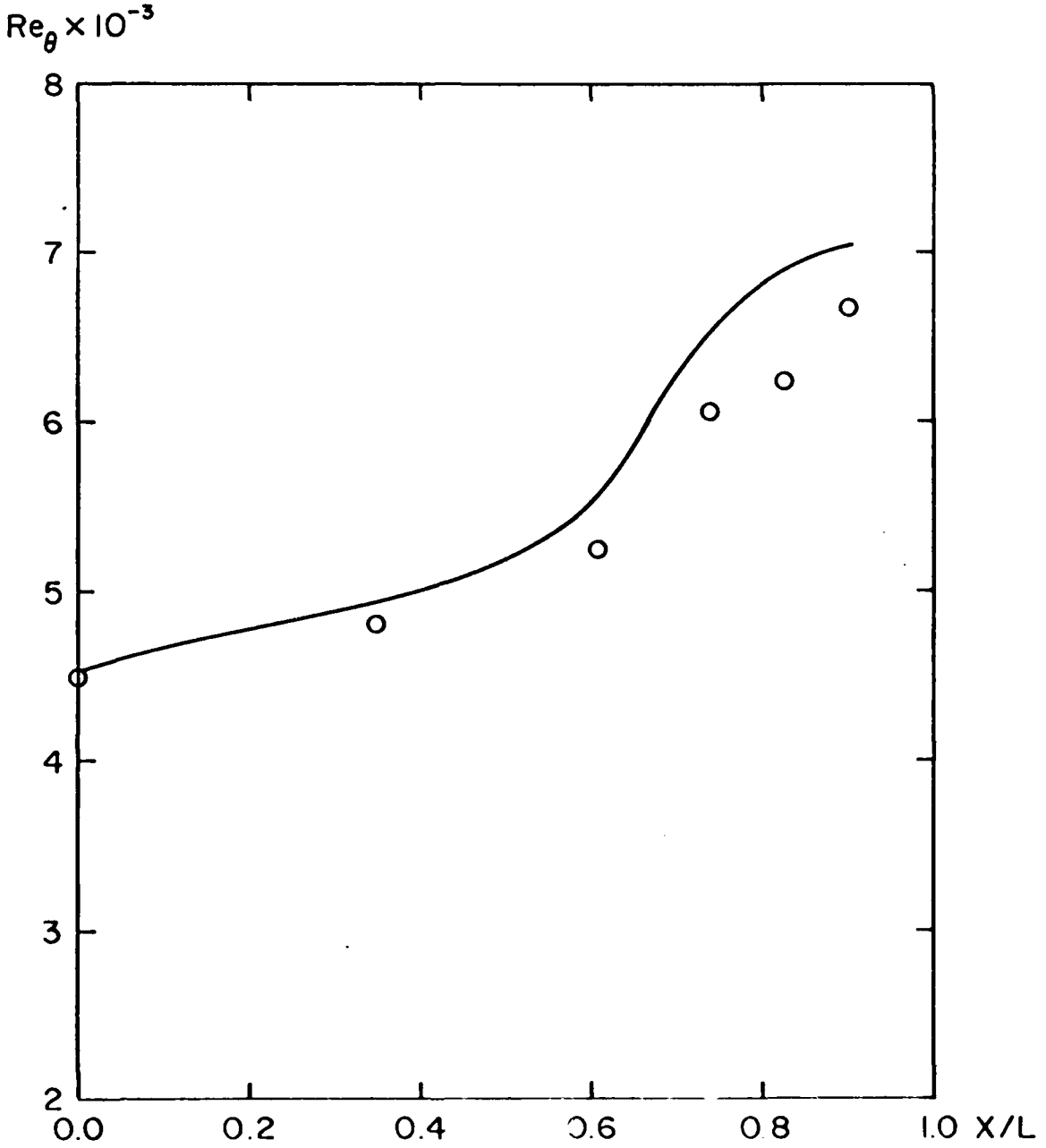

FIG. 3.6 MOMENTUM-THICKNESS REYNOLDS NUMBER ALONG STREAMLINE STARTING AT z/L = 0.14, DEFE77

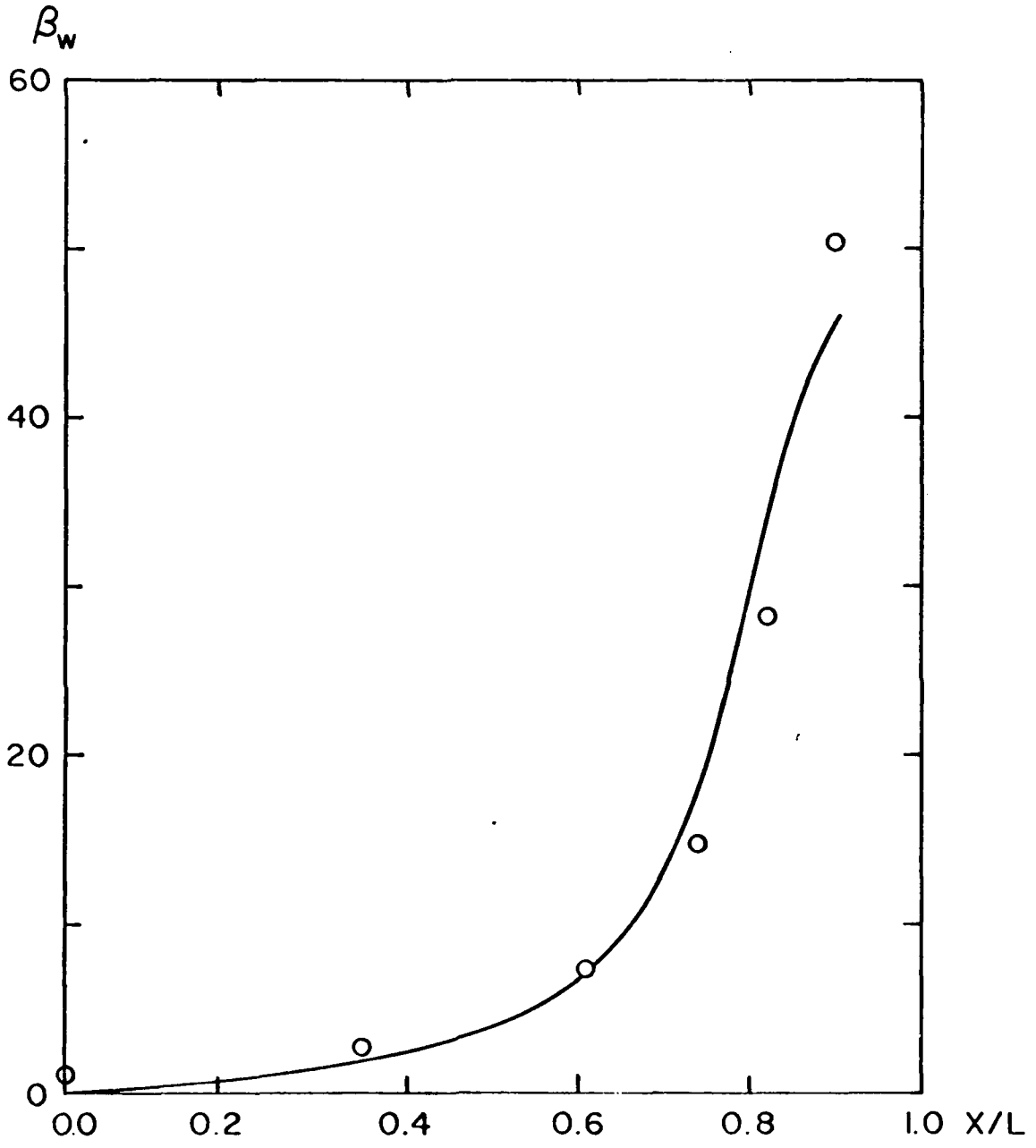

FIG. 3.7 WALL CROSSFLOW ANGLE ALONG STREAMLINE STARTING AT z/L = 0.14, DEFE77

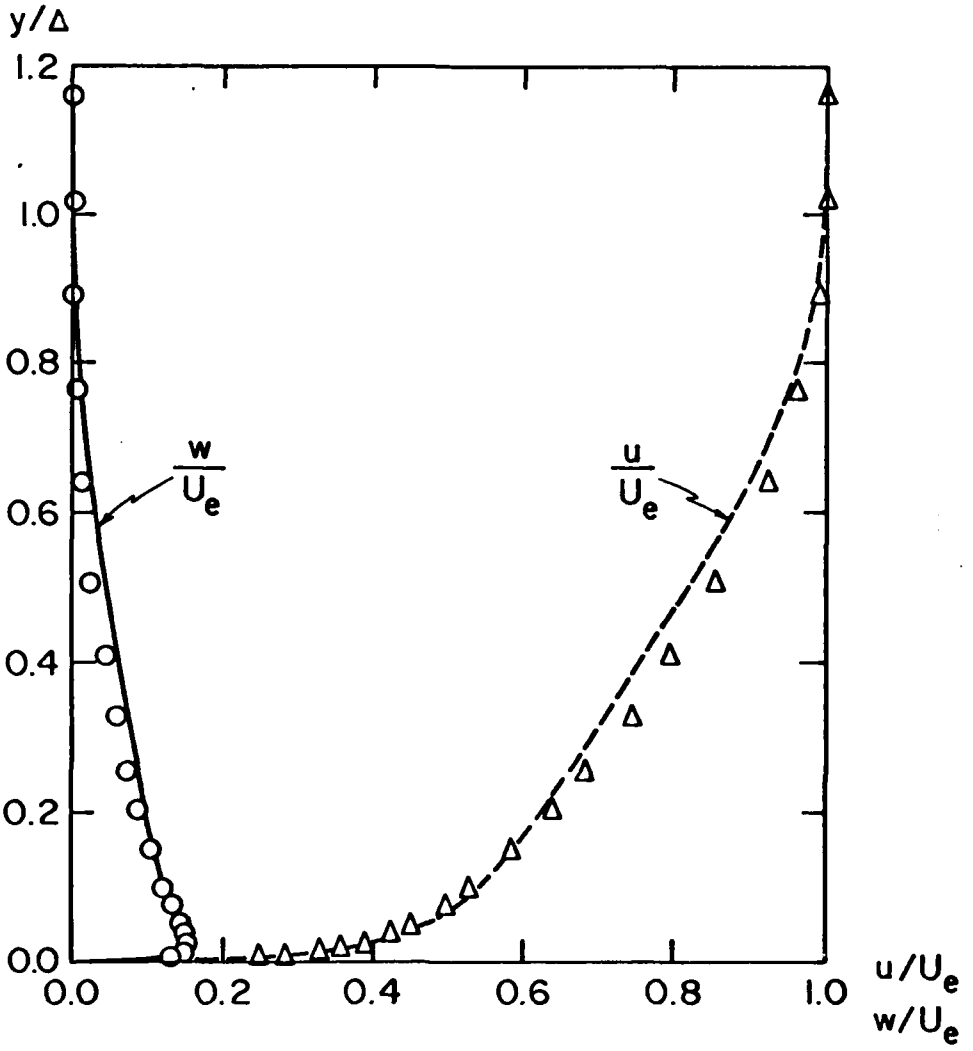

FIG. 3.8 VELOCITY PROFILES, DEFE77
x/L = 0.825, z/L = 0.162

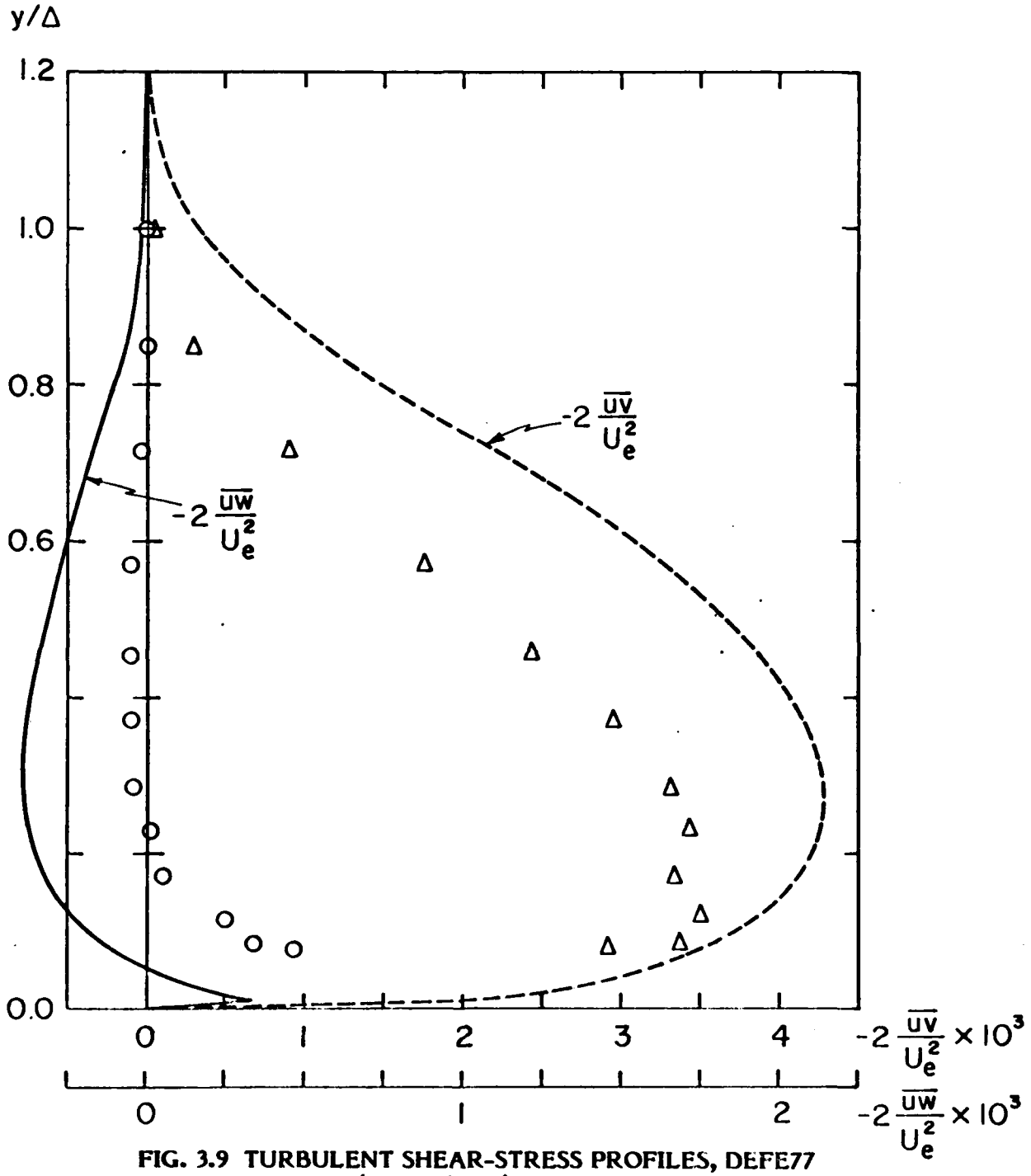

FIG. 3.9 TURBULENT SHEAR-STRESS PROFILES, DEFE77
x/L = 0.739, z/L = 0.153

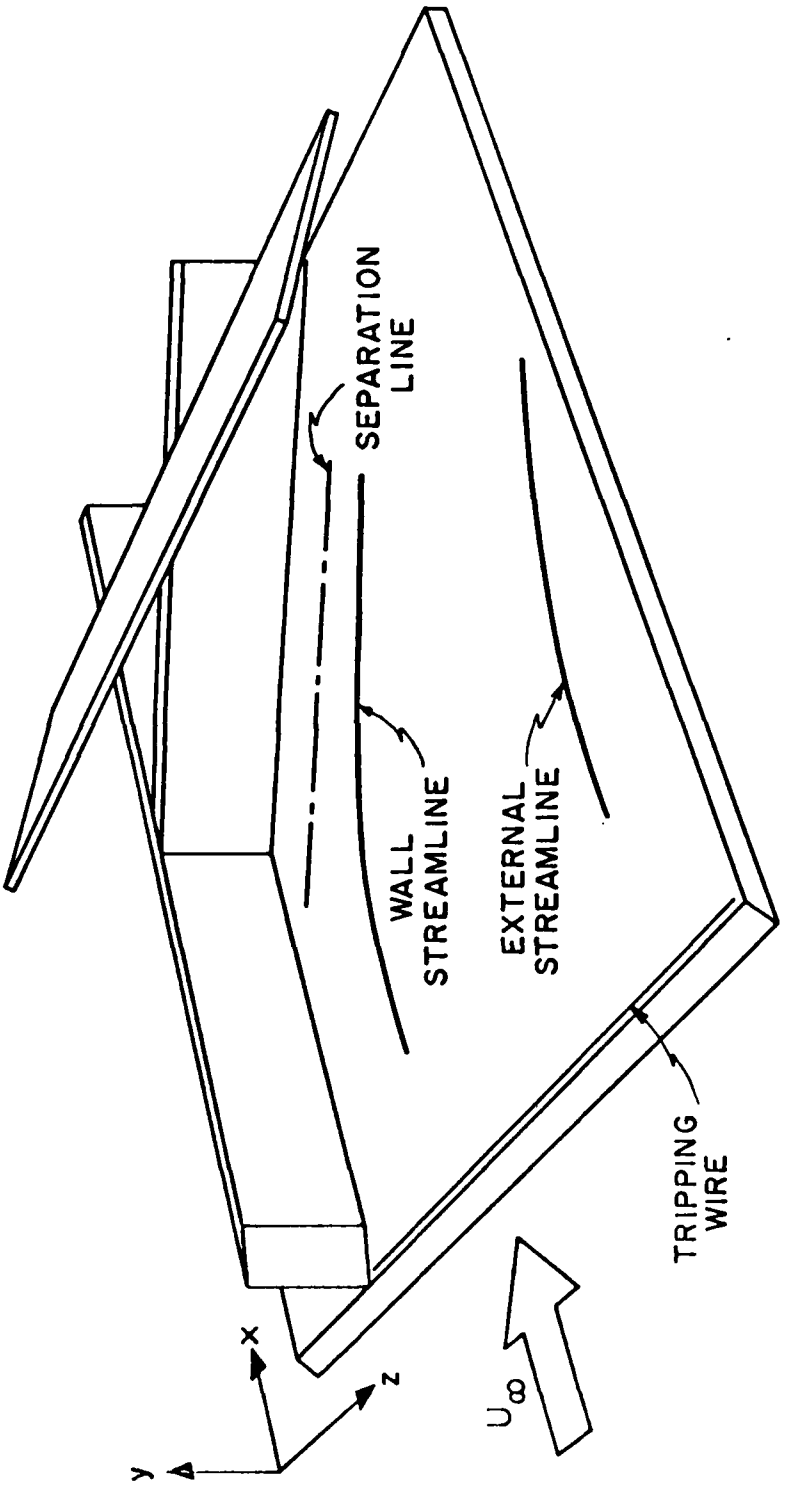

FIG. 4.1 GEOMETRY OF THE MUKR79 TEST CASE

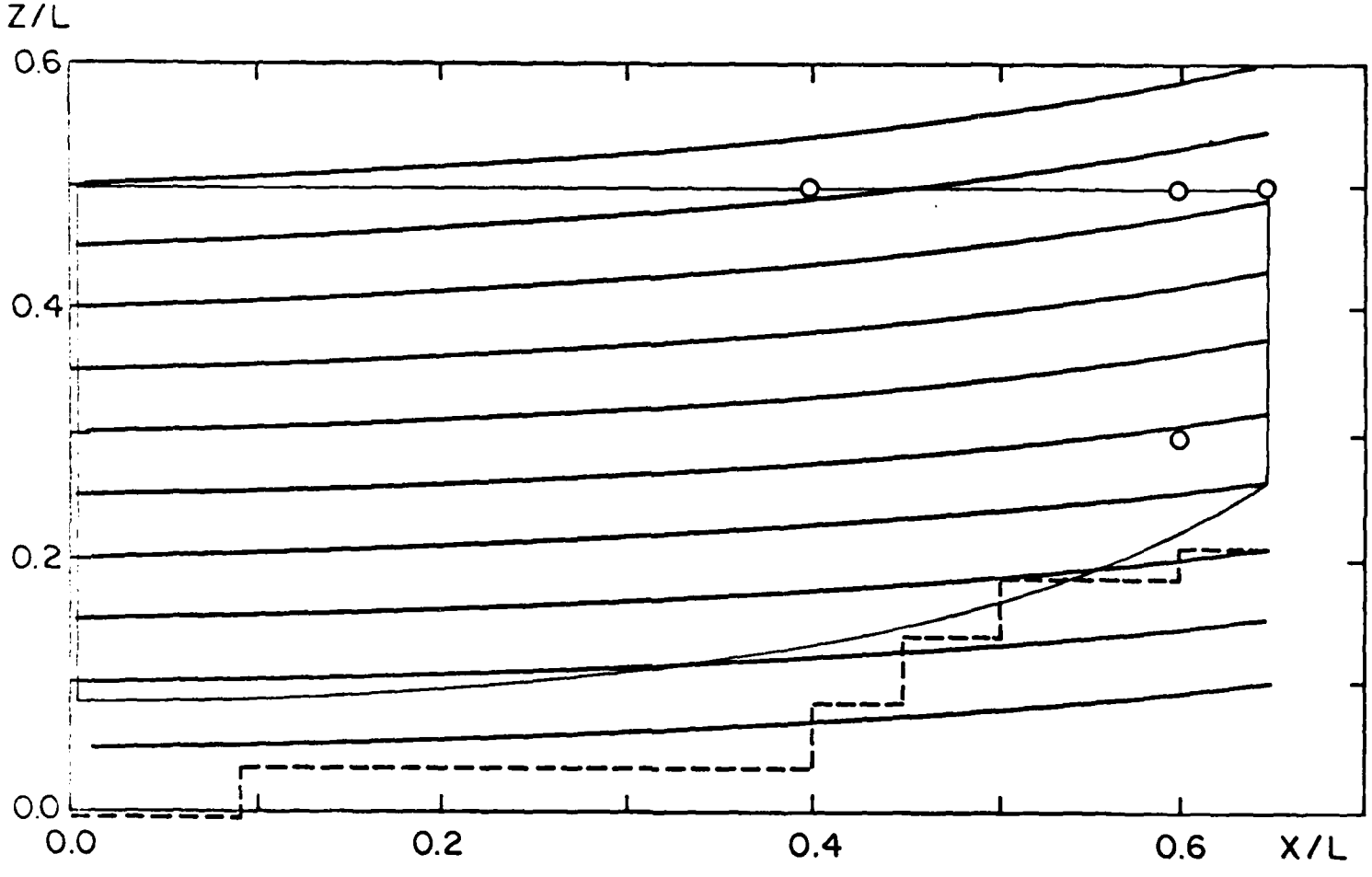

FIG. 4.2 EXTERNAL STREAMLINES FOR MUKR79 TEST CASE

EXTERNAL STREAMLINES

DOMAIN OF INFLUENCE AND COMPUTATION

REGION OF PRESSURE MEASUREMENTS

REQUIRED PROFILE OUTPUT STATION

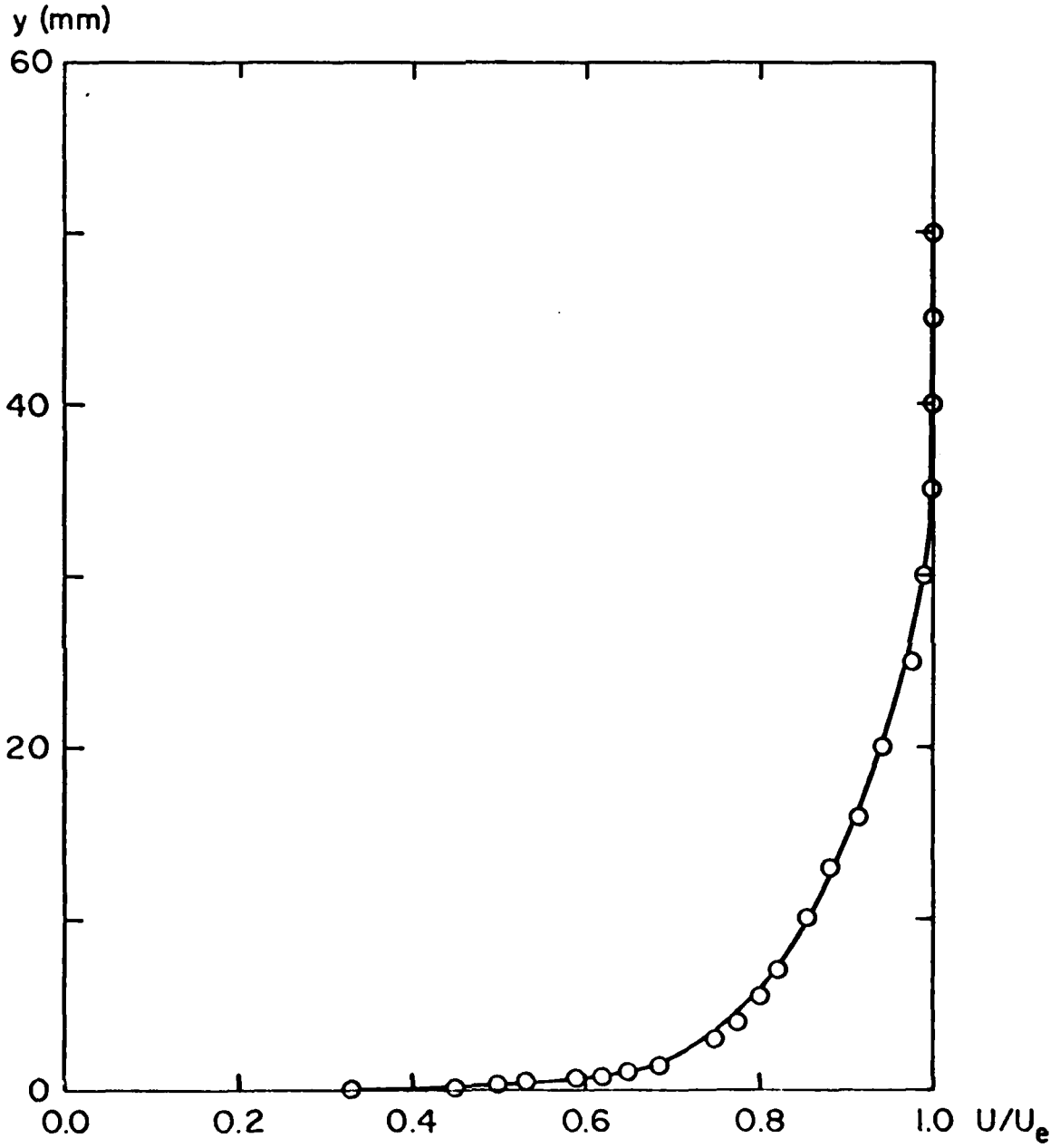

FIG. 4.3 MEASURED AND GENERATED INITIAL VELOCITY PROFILES, MUKR79

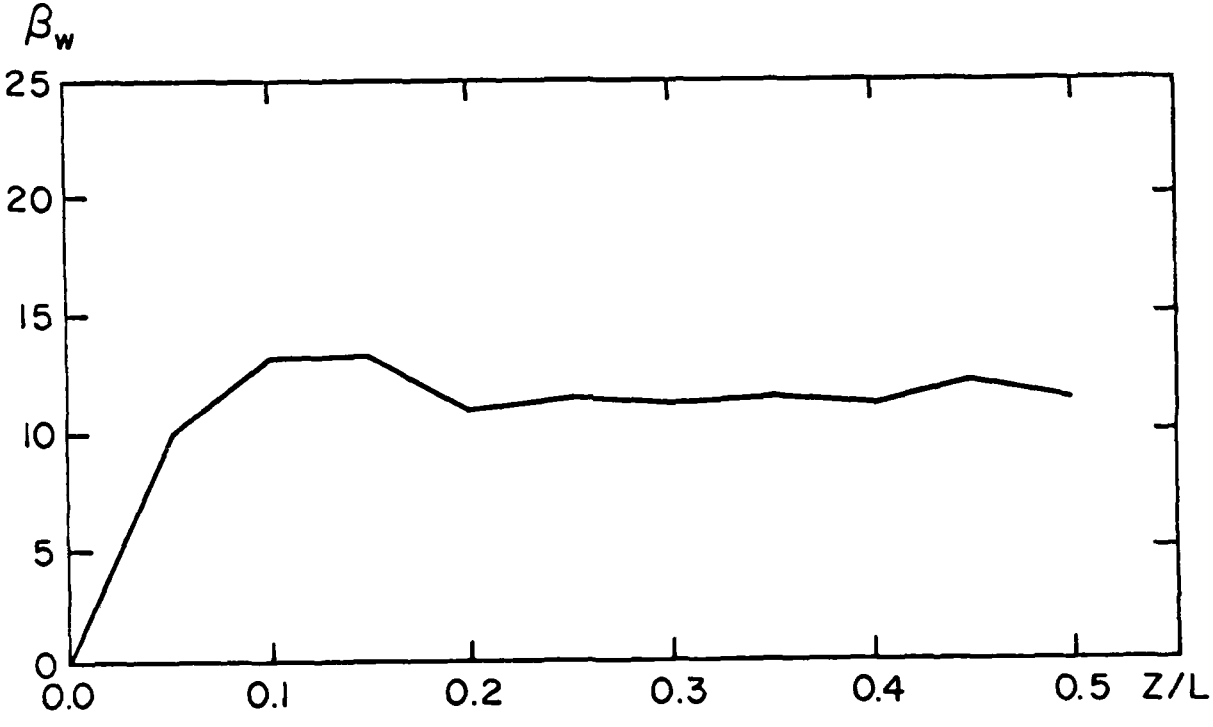

FIG. 4.4 WALL CROSSFLOW ANGLE ALONG x/L = 0.4, MUKR79

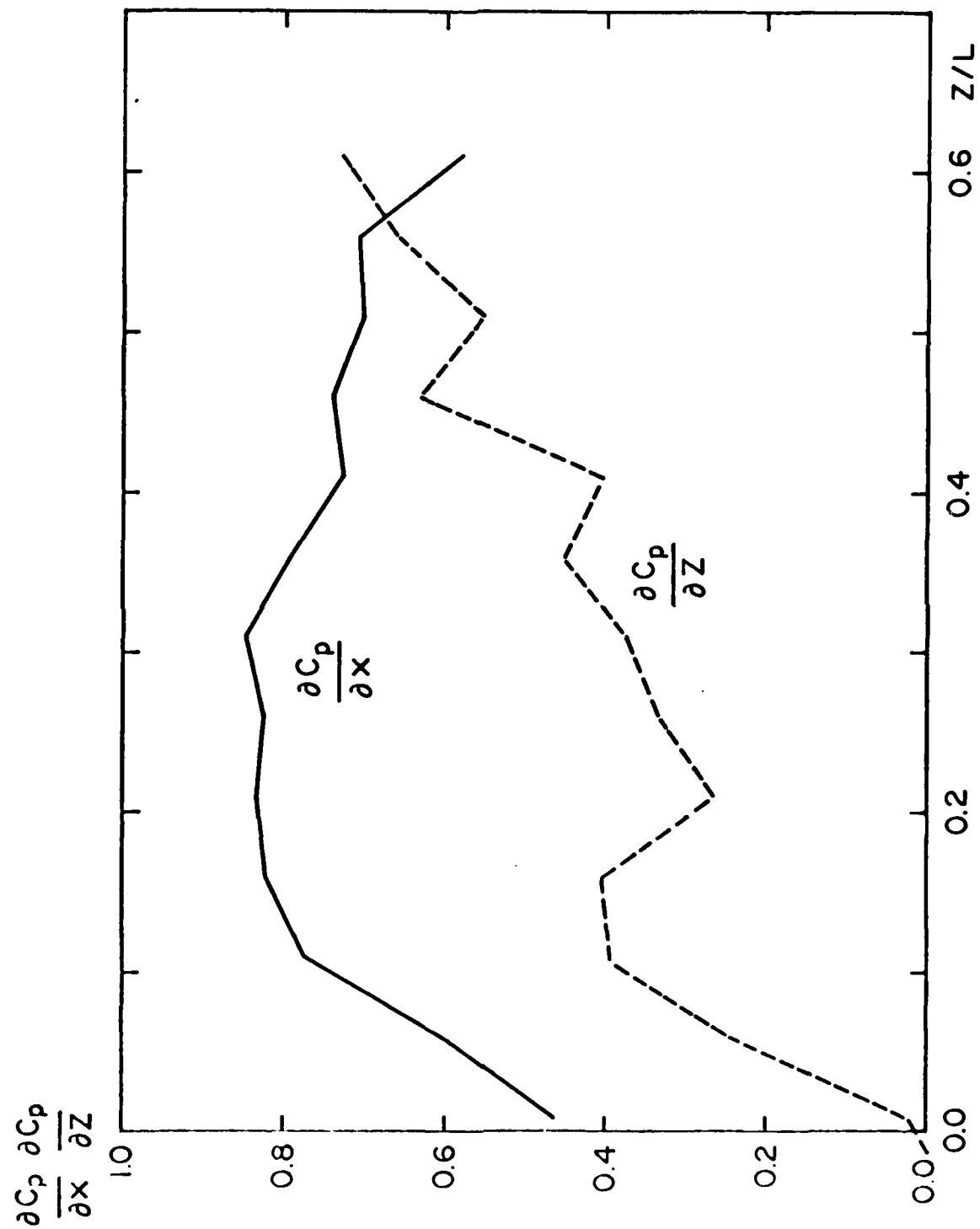

FIG. 4.5 PRESSURE GRADIENTS AT x/L = 0.4, MUKR79

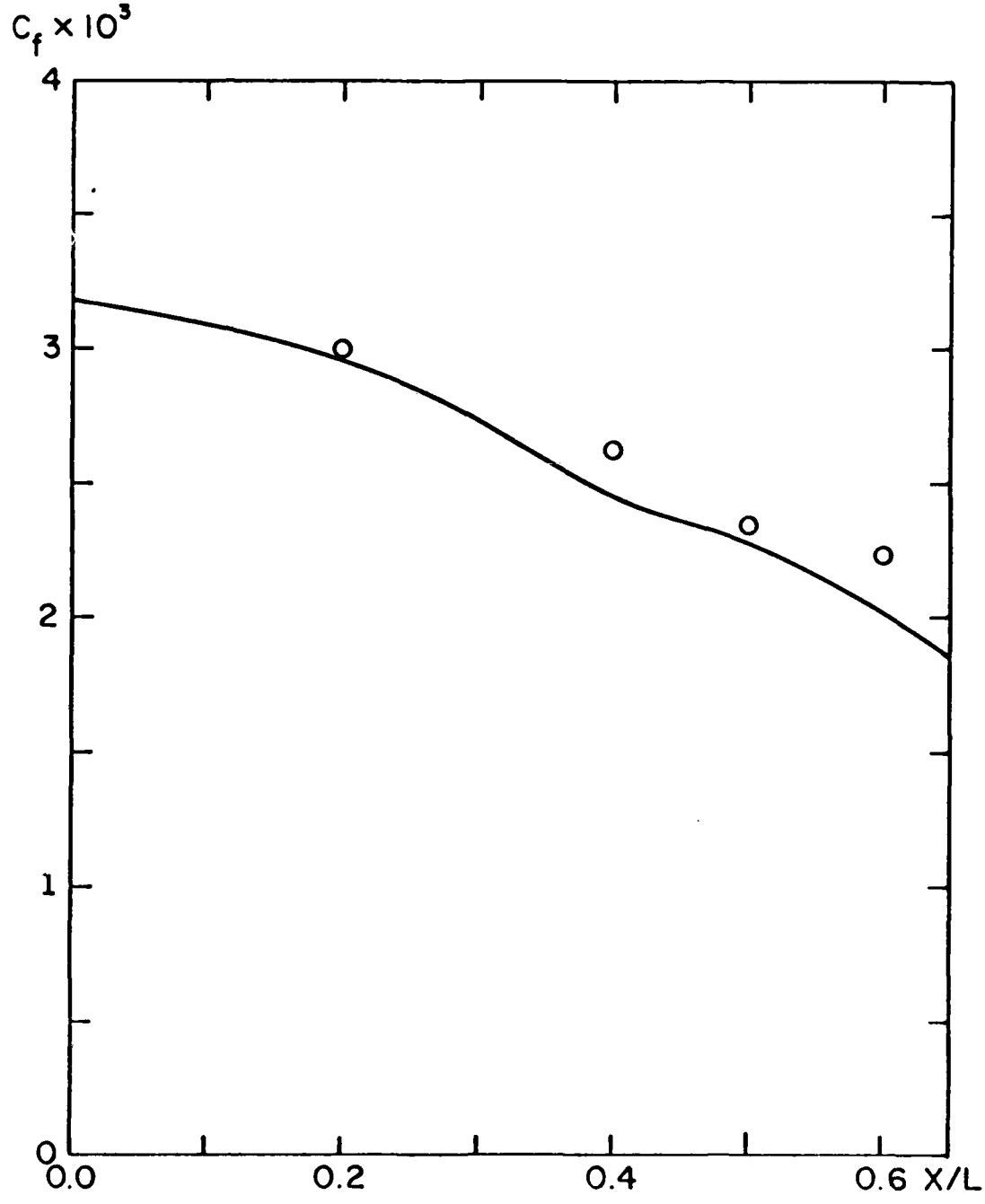

FIG. 4.6 SKIN-FRICTION COEFFICIENT ALONG z/L = 0.5, MUKR79

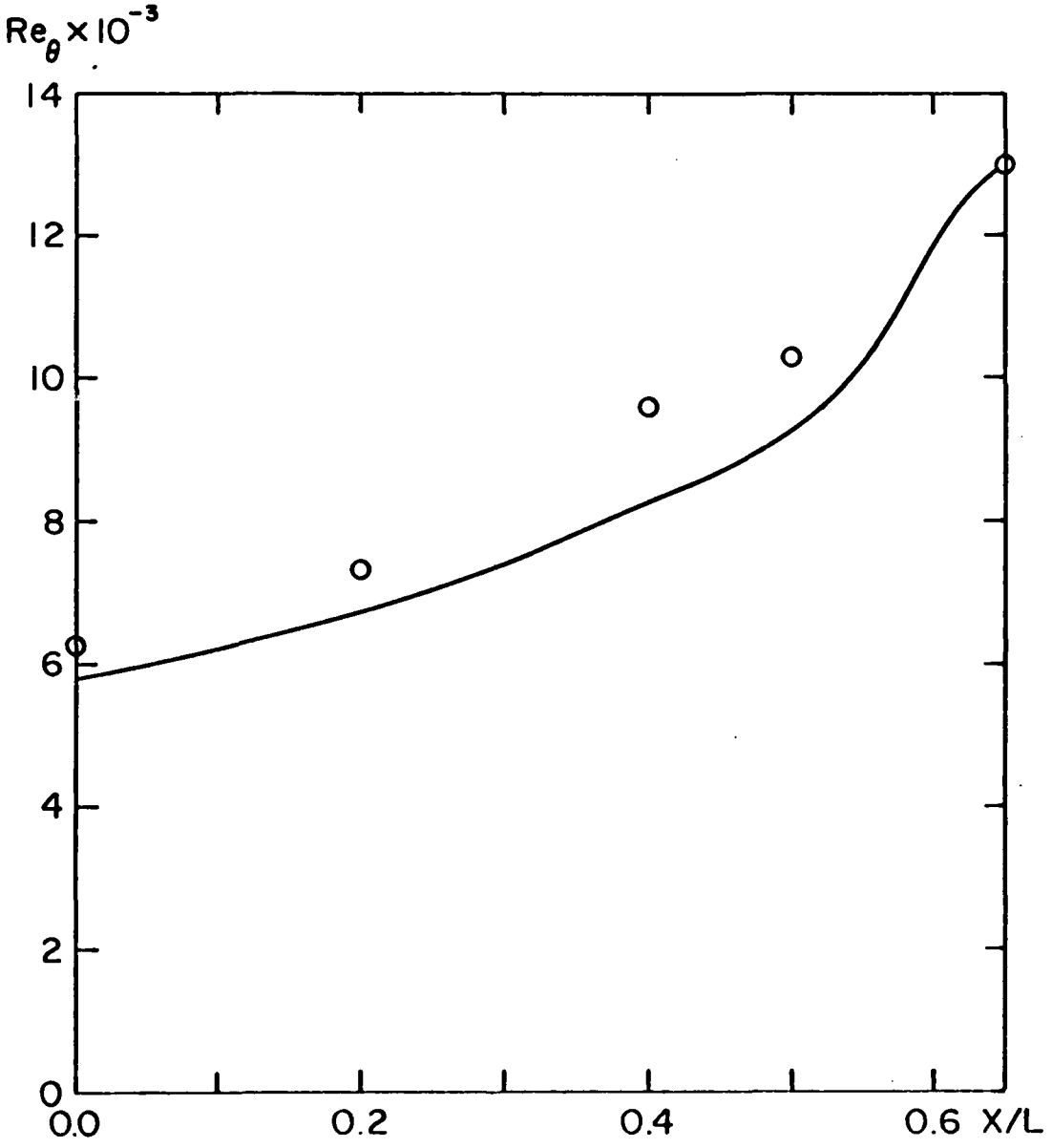

FIG. 4.7 MOMENTUM-THICKNESS REYNOLDS NUMBER ALONG z/L = 0.5, MUKR79

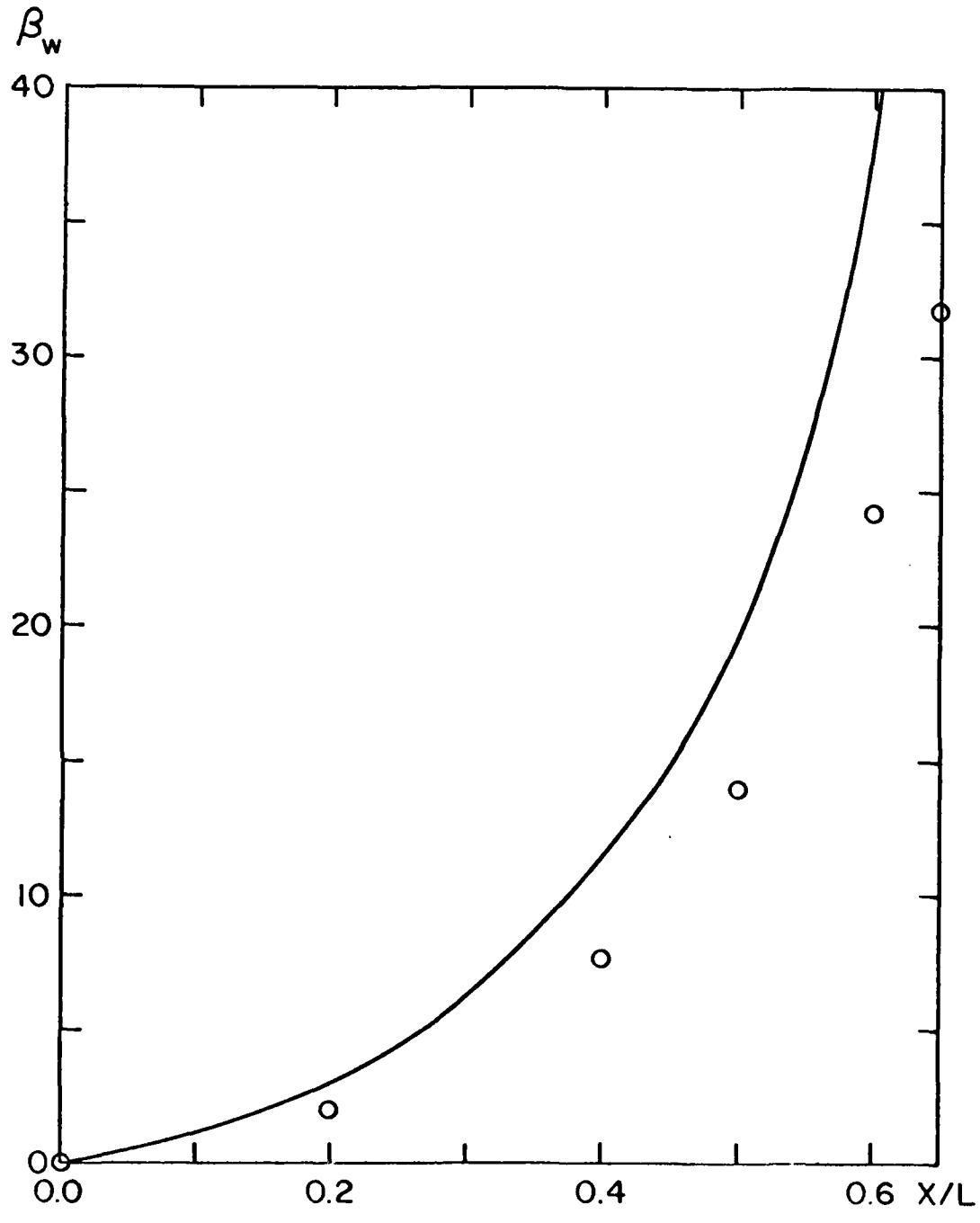

FIG. 4.8 WALL CROSSFLOW ANGLE ALONG z/L = 0.5, MUKR79

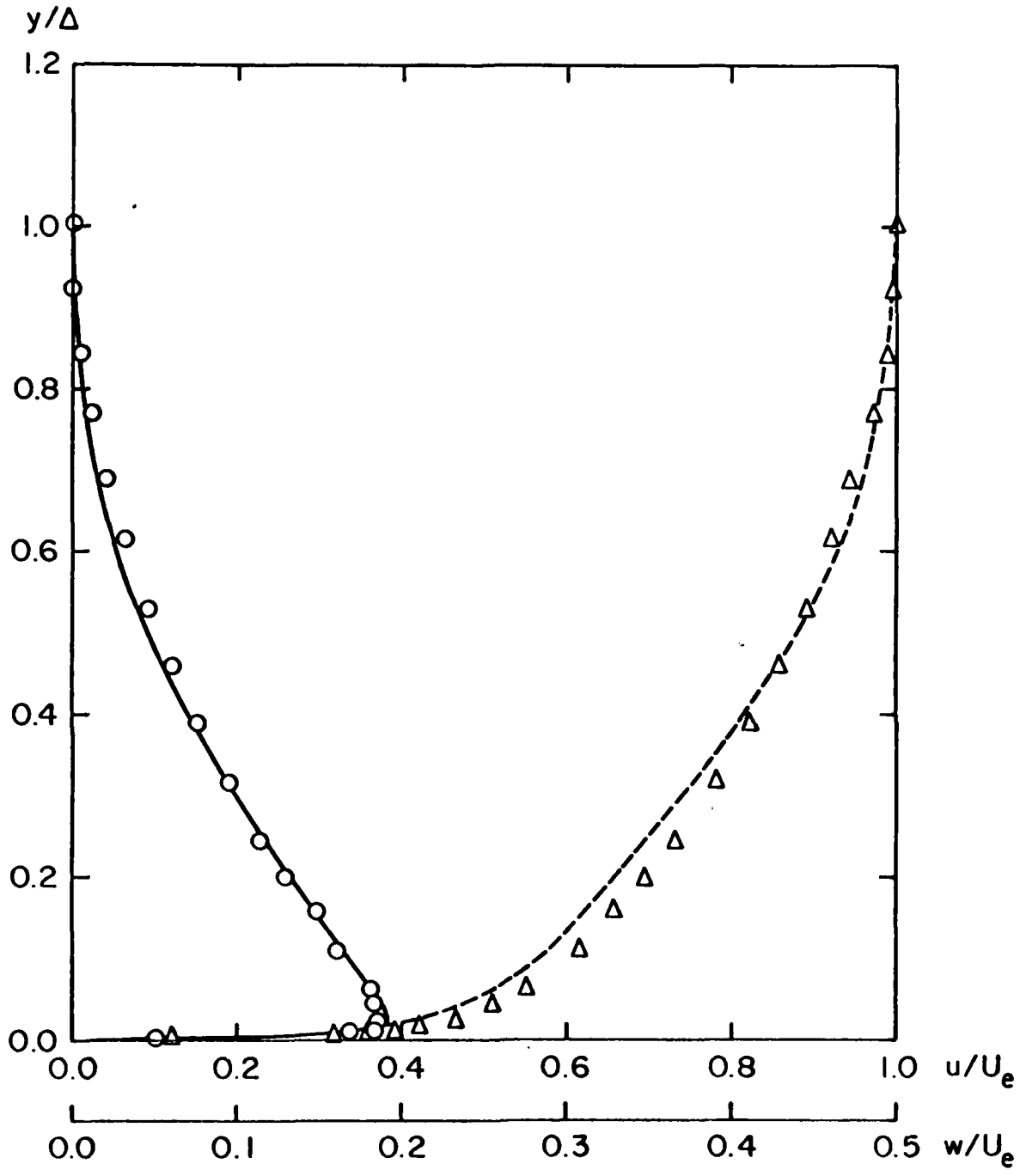

FIG. 4.9 VELOCITY PROFILES AT x/L = 0.6, z/L = 0.5, MUKR79

DISTRIBUTION LIST FOR REPORTS PREPARED UNDER THE GENERAL HYDROMECHANICS RESEARCH PROGRAM

Commander
David W. Taylor Naval Ship
R & D Center (ATTN: Code 1505)
Bldg. 19, Room 129B
Bethesda, Maryland 20084
15 Copies

Commander
Naval Sea Systems Command
Washington, D.C. 20362
ATTN: 05R22 (J. Sejd)

Commander
Naval Sea Systems Command
Washington, D.C. 20362
ATTN:55W (R. Keane, Jr.)

Commander
Naval Sea Systems Command
Washington, D.C. 20362
ATTN: 55W3 (W. Sandberg)

Commander
Naval Sea Systems Command
Washington, D.C. 20362
ATTN: 50151 (C. Kennell)

Commander
Naval Sea Systems Command
Washington, D.C. 20362
ATTN: 56X1 (F. Welling)

Commander
Naval Sea Systems Command
Washington, D.C. 20362
ATTN: 63R31 (T. Pierce)

Commander
Naval Sea Systems Command
Washington, D.C. 20362
ATTN: 55X42 (A. Paladino)

Commander
Naval Sea Systems Command
Washington, D.C. 20362
ATTN: 99612 (Library)

Director
Defense Documentation Center
5010 Duke Street
Alexandria, Va 22314
12 copies

Library of Congress
Science & Technology Division
Washington, D.C. 20540

Naval Ship Engineering Center
Norfolk Division
Combatant Craft Engr Dept
Attn: D. Blount (6660)
Norfolk, VA 23511

Naval Underwater Weapons Research
& Engineering Station (Library)
Newport, R.I. 02840

Office of Naval Research
800 N. Quincy Street
Arlington, Virginia 22217
ATTN: Dr. C.M. Lee, Code 432

Commanding Officer (L31)
Naval Civil Engineering Laboratory
Port Hueneme, CA 93043

Commander
Naval Ocean Systems Center
San Diego, CA 92152
Attn: Library

Library
Naval Underwater Systems Center
Newport, RI 02840

Research Center Library
Waterways Experiment Station
Corps of Engineers
P.O. Box 631
Vicksburg, Mississippi 39180

Charleston Naval Shipyard
Technical Library
Naval Base
Charleston, S.C. 29408

Norfolk Naval Shipyard
Technical Library
Portsmoth, VA 23709

Puget Sound Naval Shipyard
Engineering Library
Bremerton, WA 98314

Long Beach Naval Shipyard
Technical Library (246L)
Long Beach, CA 90801

Mare Island Naval Shipyard
Shipyard Technical Library (202.3)
Vallejo, CA 94592

Assistant Chief Design Engineer
for Naval Architecture (Code 250)
Mare Island Naval Shipyward
Vallejo, CA 94592

U.S. Naval Academy
Annapolis, Md 21402
Attn: Technical Library

Naval Postgraduate School
Monterey, CA 93940
Attn: Library (2124)

Study Center
National Maritime Research Center
U.S. Merchant Marine Academy
Kings Point, LI, New York 11024

The Pennsylvania State University
Applied Research Laboratory (Library)
P.O. Box 30
State College, PA 16801

Dr. B. Parkin, Director
Garfield Thomas Water Tunnel
Appliled Research Laboratory
P.O. Box 30
State College, PA

Bolt, Beranek & Newman (Library)
50 Moulton Street
Cambridge, MA 02138

Bethlehem Steel Corporation
25 Broadway
New York, New York 10004
Attn: Library-Shipbuilding

Cambridge Acoustical Associates, Inc.
54 Rindge Ave Extension
Cambridge, MA 02140

R & D Manager
Electric Boat Division
General Dynamics Corporation
Groton, Conn 06340

Gibbs & Cox, Inc. (Tech Info Control)
21 West Street
New York, New York 10006

Hydronautics, Inc. (Library)
Pindell School Rd.
Laurel, MD 20810

Newport News Shipbuilding and Dry
Dock Company (Tech. Library)
4101 Washington Ave.
Newport News, VA 23607

Mr. S. Spangler
Nielsen Engineering & Research, Inc.
510 Clyde Ave.
Mountain View, CA 94043

Society of Naval Architects and
Marine Engineers (Tech Library)
One World Trade Center, Suite 1369
New York, NY 10048

Sun Shipbuilding & Dry Dock Co.
Attn: Chief Naval A rchitect
Chester, PA 19000

Sperry Systems Management Division
Sperry Rand Corporation (Library)
Great Neck, N.Y. 10020

Stanford Research Institute
Attn: Library
Menlo Park, CA 94025

Southwest Research Institute
P.O. Drawer 28510
San Antonio, TX 78284
Attn: Applied Mech. Review
Dr. H. Abramson
2 copies

Tracor, Inc.
6500 Tracor Lane
Austin, Texas 78721

Mr. Robert Taggart
9411 Lee Highway, Suite P
Fairfax, VA 22031

Ocean Engr Department
Woods Hole Oceanographic Inc.
Woods Hole, Mass. 02543

Worcester Polytechnic Inst.
Alden Research Lab (Tech Library)
Worcester, MA 01609

Applied Physics Laboratory
University of Washington (Tech Library)
1013 N. E. 40th Street
Seattle, Washington 98105

University of California
Naval Architecture Department
Berkeley, CA 94720
4 Copies - ATTN: Profs. Webster, Paulling,
Wehausen & Library

California Institute of Technology
ATTN: Library
Pasadena, CA 91109

Engineering Research Center
Reading Room
Colorado State University
Foothills Campus
Fort Collins, Colorado 80521

Florida Atlantic University
Ocean Engineering Department
Boca Raton, Florida 33432
Attn: Technical Library

Gordon McKay Library
Harvard University
Pierce Hall
Cambridge, MA 02138

Department of Ocean Engineering
University of Hawaii (Library)
2565 The Mall
Honolulu, Hawaii 96822

Institute of Hydraulic Research
The University of Iowa
Iowa City, Iowa 52242
3 copies ATTN: Library, Landweber, Pa

Prof. O. Phillips
Mechanics Department
The John Hopkins University
Baltimore, Maryland 21218

Kansas State University
Engineering Experiment Station
Seaton Hall
Manhattan, Kansas 66502

University of Kansas
Chairman, Civil Engr Department Libra
Lawrence, Kansas 60644

Fritz Engr Laboratory Library
Department of Civil Engr
Lehigh University
Bethelehem, PA 18015

Department of Ocean Engineering
Massachusetts Institute of Technology
Cambridge, MA 02139
2 Copies: Attn: Profs. Leehey & Kerwin

Engineering Technical Reports
Room 10-500
Massachusetts Institute of Technology
Cambridge, MA 02139

St. Anthony Falls Hydraulic Laboratory
University of Minnesota
Mississippi River at 3rd Ave., S.E.
Minneapolis, Minnesota 55414
2 Copies: Attn: Dr. Austin & Library

Department of Naval Architecture
and Marine Engineering - North Camp
ATTN: Library
University of Michigan
Ann Arbor, Michigan 48109

Davidson Laboratory
Stevens Institute of Technology
711 Hudson Street
Hoboken, New Jersey 07030
Attn: Library

Applied Research Laboratory
University of Texas
P.O. Box 8029
Austin, Texas 78712

Stanford University
Stanford, California 94305
2 Copies:
Attn: Engineering Library, Dr. Street

Webb Institute of Naval Archtecture
Attn: Library
Crescent Beach Road
Glen Cove, L.I., New York 11542

National Science Foundation
Engineering Division Library
1800 G Street N.W.
Washington, D.C. 20550

Mr. John L. Hess
4338 Vista Street
Long Beach, CA 90803

Dr. Tuncer Cebeci
Mechanical Engineering Dept.
California State University
Long Beach, CA 90840

Science Applications, Inc.
134 Holiday Court, Suite 318
Annapolis, MD 21401

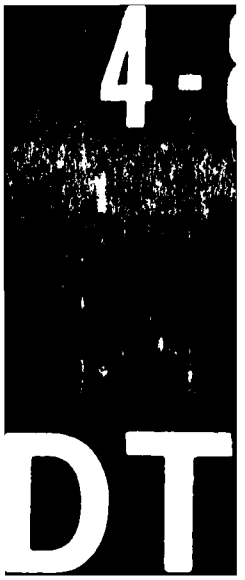
4-
DT